Maternal Pregnancy-Associated Circulating MicroRNA predictors of infant birth outcomes are Determinants of Placental Maturation

[1]Alexander M. Tseng, [1]Amanda H. Mahnke, [2,3]Alan B. Wells, [1]Nihal A. Salem, [4]Andrea M. Allan, [5]Victoria H.J. Roberts, [6]Natali Newman, [6]Nicole A.R. Walter, [6]Christopher D. Kroenke, [6]Kathleen A. Grant, [7]Lisa K. Akison, [7]Karen M. Moritz, [2,3†]Christina D. Chambers, [1†]Rajesh C. Miranda & [#]CIFASD

[1]Department of Neuroscience and Experimental Therapeutics, Texas A&M University Health Science Center, Bryan, TX, USA

[2]Clinical and Translational Research Institute, University of California San Diego, San Diego, CA, USA

[3]Department of Pediatrics, University of California San Diego, San Diego, CA, USA

[4]Department of Neurosciences, University of New Mexico, Albuquerque, NM, USA

[5]Division of Reproductive and Developmental Sciences, Oregon National Primate Research Center, Oregon Health & Science University, Portland, OR, USA

[6]Division of Neuroscience, Oregon National Primate Research Center, Oregon Health & Science University, Portland, OR, USA

[7]Child Health Research Centre and School of Biomedical Sciences, the University of Queensland, 4072, Brisbane, Australia

[†] Co-senior authors to whom correspondence should be addressed:

Dr. Rajesh Miranda,

23 email: miranda@medicine.tamhsc.edu

24 Texas A&M University Health Science Center, College of Medicine, Department of Neuroscience

25 & Experimental Therapeutics, Medical Research and Education Building 8447 Riverside

26 Parkway, Bryan, TX 77807-3260

27 Phone: 979-436-0332 Fax: 979-436-0086

28 Dr. Christina Chambers

29 email: chchambers@ucsd.edu

30 University of California San Diego, Department of Pediatrics, 9500 Gilman Drive MC 0828, La

31 Jolla, CA 92093

32 Phone: 858-246-1704, Fax: 858246-1701

33 [#]CIFASD, Collaborative Initiative on Fetal Alcohol Spectrum Disorders

34

35 Acknowledgements:

36 This research was supported by grants from the NIH, P50 AA022534 (AMA), U01 AA014835 and

37 the Office of Dietary Supplements (CDC), R24 AA019431 (KAG), R01 AA021981 (CDK), R01

38 AA024659 (RCM), F31 AA026505 (AMT) and support from National Health and Medical

39 Research Council of Australia (KMM). We thank CIFASD for intellectual support and Megan S.

40 Pope and Tenley E. Lehman for their assistance in conducting cell culture and animal studies.

41 Data on human subjects is deposited at CIFASD.org, in accordance with NIH data repository

42 guidelines.

43 **Conflict of Interest Statement**

44 The authors have declared that no conflict of interest exists.

Abstract

We previously identified 11 miRNAs which were significantly elevated in blood plasma of pregnant mothers who subsequently gave birth to infants affected by prenatal alcohol exposure (PAE, Heavily Exposed Affected: HEa) compared to those with infants who were exposed but apparently unaffected (Heavily Exposed Unaffected: HEua) or unexposed (UE). These maternal $_{HEa}$miRNAs were predicted to originate in part, as a paracrine placental signal to influence and coordinate placental epithelial-mesenchymal transition (EMT), a pathway essential for endometrial invasion and development. We now report that PAE inhibits expression of placental EMT pathway members in rodent and primate voluntary alcohol consumption models, with $_{HEa}$miRNAs collectively mediating placental EMT inhibition. To directly investigate the interaction between $_{HEa}$miRNAs and ethanol on placenta, we assessed their effects on human placental trophoblast cell lines. When administered together, $_{HEa}$miRNAs retarded trophoblast cell cycle, significantly impaired expression of core EMT pathway members, and reduced invasiveness, pointing to their collective role in modulating placental growth and invasion deficits seen with PAE. $_{HEa}$miRNAs additionally interfered with maturation-dependent intracellular calcium dynamics, while promoting syncytialization-dependent increases in placental hormone expression. Finally, a single systemic administration of the pooled murine-expressed $_{HEa}$miRNA subpopulation, to pregnant mice, decreased fetal and placental growth and inhibited expression of EMT pathway mRNA transcripts in placenta. Taken together, our data suggests that, following PAE, $_{HEa}$miRNAs interfere with placental development and may contribute to the pathology of Fetal Alcohol Spectrum Disorders.

66 **Introduction**

67 Alcohol use during pregnancy remains prevalent despite published prevention
68 guidelines (1). A recent meta-analysis determined the global prevalence of alcohol use during
69 pregnancy at 9.8% (2). Within the United States, a 2013 study found 18% of women reported
70 alcohol consumption during pregnancy, and 6.6% engaged in binge-drinking episodes, which
71 are particularly damaging to fetal development (3). In the state of Texas, we recently reported
72 an average state-wide third-trimester rate of alcohol exposure of 8.4%, with rates as high as
73 17.7% in some localities (4). These data collectively suggest that prenatal alcohol exposure
74 (PAE) is common.

75 PAE harms the developing embryo and fetus and can result in a constellation of adverse
76 infant outcomes, including craniofacial dysmorphologies, growth retardation, and
77 neurobehavioral abnormalities, collectively termed Fetal Alcohol Spectrum Disorders (FASDs)
78 (5). Estimates for the prevalence of FASDs range from 2-5% of the school age population in the
79 US and Western Europe (6) to 13.6-20.9% in South Africa (7). Estimates for the global
80 prevalence of fetal alcohol syndrome (FAS), the most severe end of the FASD continuum,
81 characterized by cranio-facial dysmorphologies, growth restriction, and CNS abnormalities,
82 range from 0.15 to 0.3% (8, 9), but are much higher in specific populations, for example, as high
83 as 5.9-9.1% in the Cape Coloured (mixed ancestry) community in South Africa (7).

84 Given the lifelong debility and economic burden associated with FASDs (10), there is an
85 urgent need to develop sensitive and specific methodologies to identify affected children early
86 in development, as well as develop interventions which can mitigate the effects of PAE on the
87 developing fetus. In 2016, we reported that elevated levels of 11 distinct microRNAs (miRNAs)

88 in 2nd and 3rd trimester maternal circulation distinguished infants who were affected by in-utero
89 alcohol exposure (Heavily Exposed Affected: HEa) from those who were apparently unaffected
90 at birth by PAE (Heavily Exposed Unaffected: HEua), or those who were unexposed (UE) (11) .
91 We predicted that these HEamiRNAs (MIMAT0004569 [hsa-miR-222-5p], MIMAT0004561 [hsa-
92 miR-187-5p], MIMAT0000687 [hsa-mir-299-3p], MIMAT0004765 [hsa-miR-491-3p],
93 MIMAT0004948 [hsa-miR-885-3p], MIMAT0002842 [hsa-miR-518f-3p], MIMAT0004957 [hsa-
94 miR-760], MIMAT0003880 [hsa-miR-671-5p], MIMAT0001541 [hsa-miR-449a], MIMAT0000265
95 [hsa-miR-204-5p], MIMAT0002869 [has-miR-519a-3p]) in addition to being biomarkers of infant
96 outcome following PAE, influence signaling pathways crucial for early development, particularly
97 the epithelial-mesenchymal transition (EMT) pathway (11).
98 Placental development involves maturation of the cytotrophoblasts at the tip of
99 anchoring villi into invasive extravillous trophoblasts, as well as fusion of cytotrophoblasts into
100 multinucleate, hormone-producing syncytiotrophoblasts (12). Maturation into extravillous
101 trophoblasts, which invade the maternal decidua and remodel the uterine spiral arteries into
102 low-resistance high-flow vessels that enable optimal perfusion for nutrient and waste
103 exchange, requires cytotrophoblasts to undergo EMT (13). Impaired placental EMT, as well as
104 orchestration of the opposing mesenchymal-epithelial transition pathway, has been found in
105 conditions resulting from placental malfunction, primarily preeclampsia (14-19). While there
106 have been no previous studies directly investigating the effects of PAE on placental EMT, a
107 rodent study demonstrated that PAE, during a broad developmental window, reduced the
108 number of invasive trophoblasts within the mesometrial triangle, a region of the uterine horn
109 directly underlying the decidua (20). Furthermore, both human and rodent studies have found

110 PAE disrupts placental morphology, and interferes with cytotrophoblast maturation, as with
111 preeclampsia (21-24). Disrupted trophoblast maturation, seen in these conditions, is associated
112 with aberrant expression of placental hormones, primarily human chorionic gonadotropin
113 (hCG) (25-28). Our study is the first to report that PAE interferes with expression of core
114 placental EMT pathway members. We also provide evidence that a group of circulating
115 maternal miRNAs, HEamiRNAs, which predict adverse infant outcomes due to PAE, mediate
116 some of PAE's effects and interfere with EMT and cytotrophoblast maturation.
117

118 **Results**

119 HEamiRNAs are implicated in placental-associated pathologies

120 Outside of our report that elevated HEamiRNA levels predict infant outcomes following
121 PAE, few other studies have investigated expression of these miRNAs in the context of PAE or
122 other potentially toxic prenatal exposures (Figure 1A) (29-36). Given our prediction that
123 HEamiRNAs interfere with signaling pathways governing fetal and placental development (11),
124 we conducted a literature review of reports on HEamiRNA levels in gestational pathologies
125 which, as with PAE, include aberrant placentation as an etiological factor (37-39). Surprisingly,
126 placental and plasma levels of 8 out of 11 of these HEamiRNAs were significantly dysregulated in
127 one or more of these gestational pathologies with expression of the majority of these 8 miRNAs
128 altered in both fetal growth restriction and preeclampsia (Figure 1B) (33, 34, 36, 40-57), both of
129 which are characterized by poor placental invasion as an etiological factor (58-64).

130 HEamiRNAs explain variance in infant growth outcomes due to PAE

131 Given the association of individual HEamiRNAs with gestational pathologies, we sought to
132 determine if circulating HEamiRNAs levels could explain the variance in sex and gestational age-
133 adjusted neonatal height, weight and head circumference in our Ukrainian birth cohort, which
134 are growth measures sensitive to in utero environment (65). We found that 8 of the HEamiRNAs,
135 each significantly explained between 7 to 19% of infant variation in these growth measures
136 (Table 1). Furthermore, 7 of these miRNAs were also associated with fetal growth restriction
137 and preeclampsia as identified by our literature review. Additionally, only 1 of the 3 miRNAs not
138 previously-reported to be associated with gestational pathologies was correlated with
139 measures of fetal growth and development in our dataset (Figure 1B). Interestingly, a

140 multivariate statistical regression model that accounted for levels of all 11 $_{HEa}$miRNAs together,
141 explained a far greater proportion of infant variance, between 24-31%, in all three growth
142 measures than accounting for them individually (Supplementary Table 2).
143
144 $_{HEa}$miRNAs are transcribed preferentially in the placenta
145 Data extracted from publicly available gene expression profiling datasets (66) show that
146 $_{HEa}$miRNAs as well as their unprocessed precursor transcripts, $_{HEa}$pri-miRNAs, are enriched in
147 placenta compared to other tissues, suggesting that the placenta itself transcribes these
148 miRNAs and may be a significant contributory tissue to maternal circulating $_{HEa}$miRNAs (Figures
149 1C and D). Since chorionic villi are immersed in maternal blood, it is possible that the placenta is
150 both a source and a target of maternal $_{HEa}$miRNAs. Moreover, since $_{HEa}$miRNAs are also
151 associated with gestational pathologies caused by poor placental invasion, these $_{HEa}$miRNAs
152 may also constitute an intra-placental paracrine signal to coordinate the (mal)adaptive
153 response of tissues to PAE. We therefore assessed in rodent and primate models, whether PAE
154 could result in impaired EMT, and if $_{HEa}$miRNAs could explain the effects of PAE on placental
155 EMT-associated gene expression.
156
157 $_{HEa}$miRNAs moderate PAE's effects on EMT pathway members
158 EMT, in trophoblasts, is characterized by the disappearance of epithelial markers like E-
159 Cadherin and the appearance of the mesenchymal markers like the intermediate filament,
160 vimentin, a process that is controlled by the expression of key mesenchymal determination
161 transcription factors, Snail1 and 2 and TWIST, as extensively described (13, 17, 18, 67-70).

162 These five markers have been used extensively to assess EMT in a variety of model systems, so
163 our studies utilized these markers to assess the effects of alcohol and $_{HEa}$miRNAs on trophoblast
164 EMT.

165 In the first analysis, using a murine model of PAE that mimicked moderate to binge-type
166 alcohol consumption throughout early and mid-pregnancy, we fractionated GD14 placenta into
167 three zones: the cytotrophoblast and syncytiotrophoblast rich labyrinth zone, the glycogen and
168 spongiotrophoblast rich junctional zone, and the decidual zone comprising the endometrial
169 contribution to the placenta (Figure 2A). Multivariate analysis of variance (MANOVA) for
170 expression of these five core genes in the EMT pathway within placental trophoblasts, revealed
171 a significant effect of ethanol exposure on EMT pathway member expression selectively within
172 the labyrinth zone (Pillai's trace statistic, $F_{(5,21)}=6.85$, $p<0.001$, Figure 2B) but not within the
173 junctional or decidual zones. Post-hoc univariate ANOVA indicated ethanol exposure specifically
174 elevated *CDH1* ($F_{(1,25)}=7.452$, $p=0.011$), which encodes epithelial E-Cadherin, whereas
175 expression of the pro-mesenchymal transcription factor *SNAI1* was significantly reduced
176 ($F_{(1,25)}=21.022$, $p=0.0001$). We also observed a significant interaction between fetal sex and PAE
177 on expression of *SNAI2* ($F_{(1,25)}=2.18$, $p=0.047$) and a trend towards decreased expression of the
178 terminal mesenchymal marker *VIM* (Vimentin, $F_{(1,25)}=2.749$, $p=0.11$), while there was no effect
179 on *TWIST* expression (Figures 3A-3E). Consistent with our gene expression data, E-Cadherin
180 protein levels were significantly elevated in the labyrinth zone of PAE placenta ($F_{(1,24)}=31.63$,
181 $p=0.0005$), while not in the junctional or decidual zones (Figure 3F and Supplementary Figures
182 3A and B). However, when we controlled for expression of the 8 mouse homologues of
183 $_{HEa}$miRNAs as a covariate, using multivariate analysis of covariance (MANCOVA), ethanol's effect

184 on EMT became marginally nonsignificant (Pillai's trace, $F_{(5,21)}$=2.713, p=0.068) (Figure 2C),
185 suggesting that these miRNAs partially mediate effects of PAE on EMT pathway members in
186 mice. Interestingly, PAE limited to the peri-conceptional period in rats also influenced
187 expression of EMT core transcripts (Supplementary Figures 2B and 4A-4E).

188 To determine if PAE's effects on EMT pathway members in placenta are broadly
189 conserved throughout mammalian evolution, we adopted a non-human primate (macaque)
190 model of moderate to binge-type alcohol consumption. Placental tissues were isolated from
191 GD85, GD110, and GD 135 placenta (Figure 2D), which spans the human equivalent of mid-
192 second to mid-third trimester (Supplementary Figure 2C). There was a significant effect of
193 ethanol exposure on expression of core EMT mRNA transcripts by MANOVA (Pillai's trace
194 statistic, $F_{(4,9)}$=4.229 p=0.045, Figure 3B). Consistent with our findings in mouse, post-hoc
195 univariate ANOVA indicated that in primate placenta, ethanol exposure significantly increased
196 *CDH1* expression ($F_{(1,12)}$=4.866, p=0.048) whereas *VIM* expression was significantly reduced
197 ($F_{(1,12)}$=12.782, p=0.0004), suggesting that, as in the mouse, PAE also impairs EMT in the primate
198 placenta. Interestingly, there was no effect on *SNAI2* or *TWIST* expression (Figures 3G-3J). As in
199 mice, accounting for expression of $_{HEa}$miRNAs together as a covariate abolished the significant
200 effect of PAE on EMT, though to a greater degree than mice (Pillai's trace, $F_{(1,1)}$=1.605, p=0.425,
201 Figure 2E). Interestingly, accounting for expression of individual $_{HEa}$miRNAs did not explain the
202 effects of PAE on placental EMT, suggesting that $_{HEa}$miRNAs act in concert to mediate the effect
203 of PAE on EMT in primate placenta (Figure 2F).

204 Collectively, our data suggests PAE induced impairment of EMT in the trophoblastic
205 compartment of placentae is conserved between rodents and non-human primates and that

206 $_{HEa}$miRNAs, particularly in primates, may moderate the effect of PAE on placental EMT.
207 Consequently, subsequent studies focused on the collective role of $_{HEa}$miRNAs, either on basal
208 or on alcohol-influenced placental trophoblast growth, invasion, and the maturation of
209 physiological function.
210
211 <u>$_{HEa}$miRNAs impair EMT pathway member expression in a model of human cytotrophoblasts</u>
212 To investigate whether $_{HEa}$miRNAs collectively interfere with the EMT pathway, as
213 suggested by our in vivo data, we measured expression of core members of the EMT pathway
214 after transfecting $_{HEa}$miRNA mimics and antagomirs into BeWO cytotrophoblasts.
215 Cytotrophoblasts normally undergo EMT to become invasive trophoblasts, which we also
216 modelled using the HTR8 human extravillous trophoblast cell line. We initially overexpressed
217 each of the 11 $_{HEa}$miRNAs individually, to determine whether any of them could alter mRNA
218 transcripts for EMT pathway members. However, we did not observe any significant effects due
219 to overexpression of individual miRNAs (Supplementary Figure 5), consistent with our findings
220 in the primate PAE model that individual miRNAs did not explain the effects of ethanol on EMT.
221 In contrast, transfection of pooled $_{HEa}$miRNAs into cytotrophoblasts significantly increased *CDH1*
222 expression ($F_{(1,36)}$=30.08, $p<0.0001$). Interestingly, expression of the pro-mesenchymal
223 transcription factors *TWIST* and *SNAI1* were also significantly reduced, but only in the context of
224 concomitant 320 mg/dL ethanol treatment, pointing to an interaction effect between
225 $_{HEa}$miRNAs and ethanol ($F_{(1,36)}$= 5.650 and 5.146 respectively, p=0.023 and p=0.029, Figures 4A-
226 D). Consistent with our qPCR data, transfection of $_{HEa}$miRNAs also significantly increased E-
227 cadherin protein expression ($F_{(1,20)}$=33.86, $p<0.0001$, Figure 4E). We were unable to detect

228 *SNAI2* transcript expression or vimentin protein expression in these cells, consistent with
229 previous reports (71).
230 Whereas transfection of $_{HEa}$miRNA mimics increased *CDH1* expression, transfection of
231 pooled antagomirs to $_{HEa}$miRNAs, significantly reduced CDH1 expression, only in the context of
232 320 mg/dL ethanol co-exposure (post-hoc Tukey's HSD, p=0.005), consistent with an overall
233 statistically significant interaction effect between ethanol exposure and $_{HEa}$miRNA inhibition
234 ($F_{(1,36)}$=13.51, p=0.0008, Figure 4F). However, expression of *TWIST* was also decreased in this
235 context and there was no significant difference in E-Cadherin protein expression relative to the
236 control (Figure 4G-J). Thus, our data suggest that, increasing $_{HEa}$miRNA levels impairs EMT
237 pathway members in cytotrophoblasts whereas inhibiting their action has a more restricted
238 effect on EMT pathway members.
239
240 <u>$_{HEa}$miRNAs impair EMT member expression in a model of human extravillous trophoblasts</u>
241 We next investigated the effect of $_{HEa}$miRNAs on EMT in HTR-8/SVneo extravillous
242 trophoblast-type cells. Transfecting pooled $_{HEa}$miRNA mimics into extravillous trophoblasts
243 significantly decreased *VIM* expression ($F_{(1,36)}$=28.43, p<0.0001). Expression of pro-
244 mesenchymal transcription factors *SNAI2* was also reduced ($F_{(1,36)}$= 64.88 respectively,
245 p<0.0001). As with cytotrophoblasts, expression of SNAI1 and *TWIST* were reduced only with
246 320 mg/dL ethanol co-exposure (post-hoc Tukey's HSD, p =0.027 and p<0.0001 respectively)
247 indicating an interaction effect ($F_{(1,36)}$=4.21 and 5.18, p=0.048 and 0.029 respectively, Figures
248 5A-D). Consistent with our qPCR data, Vimentin protein expression was also significantly
249 reduced ($F_{(1,20)}$=9.535, p=0.006, Figure 5E). Interestingly, there was also a main effect of alcohol

250 exposure on decreasing vimentin protein expression ($F_{(1,20)}$=7.303, p=0.014). We were unable to
251 detect expression of *CDH1* transcript, or its E-Cadherin protein product, in extravillous
252 trophoblasts, consistent with previous reports (71).

253 In contrast to $_{HEa}$miRNA mimics, transfecting pooled antagomirs significantly increased
254 *VIM* expression ($F_{(1,35)}$=42.56, p<0.0001). Likewise, there were interaction effects for *SNAI1* and
255 *SNAI2* ($F_{(1,35)}$=10.31 and 4.86, p=0.01 and p=0.034 respectively), whereby antagomir
256 transfection increased expression of Snai2 in the context of 320mg/dL ethanol co-exposure
257 (post-hoc Tukey's HSD, p<0.0001) and Snai1 under basal conditions (post-hoc Tukey's HSD,
258 p<0.0001)(Figures 5F-I). Despite our qPCR data, we did not observe significant differences in
259 vimentin protein expression between treatment groups (Figure 5J). Collectively, our data
260 indicate that increased trophoblastic $_{HEa}$miRNA levels favors an epithelial phenotype, whereas
261 inhibiting their action promotes a mesenchymal phenotype.

262

263 <u>Antagomirs prevent $_{HEa}$miRNAs' inhibition of EMT pathway members</u>

264 We next investigated if pretreating trophoblasts with pooled $_{HEa}$miRNA antagomirs could
265 prevent inhibition of the EMT pathway caused by transfecting $_{HEa}$miRNA mimics. *CDH1*
266 expression in cytotrophoblasts transfected with control antagomir, and subsequently
267 transfected with control mimic, was not significantly different from those transfected with
268 $_{HEa}$miRNA antagomirs and $_{HEa}$miRNA mimics. However, *CDH1* was significantly elevated in
269 cytotrophoblasts transfected with control antagomir and $_{HEa}$miRNA mimics (post-hoc Tukey's
270 HSD, n=10 samples per group, p=0.004). Likewise, cells pre-transfected with $_{HEa}$miRNA
271 antagomirs had significantly higher *SNAI1* and *VIM* expression than those pre-transfected with

272 control antagomir and subsequently transfected with $_{HEa}$miRNA mimics (post-hoc Tukey's HSD,
273 n=10 samples per group, p=0.007 and p<0.0001 respectively) (Figure 6A-D).
274 Furthermore, *VIM* expression in extravillous trophoblasts pre-transfected with control
275 antagomir, and subsequently transfected with control mimic, was not significantly different
276 from those transfected with $_{HEa}$miRNA antagomirs and $_{HEa}$miRNA mimics. However, *VIM*, *SNAI1*,
277 and *SNAI2* expression were significantly reduced in cytotrophoblasts transfected with control
278 antagomir and $_{HEa}$miRNA mimics (post-hoc Tukey's HSD, n=10 samples per group, p<0.0001,
279 Figure 6E-H). Thus, our data suggest that pretreating cells with $_{HEa}$miRNA antagomirs prevents
280 inhibition of EMT pathway members resulting from transfection with $_{HEa}$miRNA mimics in
281 cytotrophoblasts and extravillous trophoblasts.
282
283 <u>$_{HEa}$miRNAs impair extravillous trophoblast invasion</u>
284 Functionally, inhibition of the EMT pathway should reduce trophoblast invasiveness.
285 Thus, we performed a transwell invasion assay using HTR8 extravillous trophoblasts transfected
286 with $_{HEa}$miRNA mimics and antagomirs. While ethanol exposure by itself did not impair
287 trophoblast invasion (Supplementary Figure 6), there was a marginally significant interaction
288 effect between ethanol exposure and $_{HEa}$miRNA mimic transfection ($F_{1,28}$=3.418, p=0.075).
289 Thus, a planned comparison indicated that transfection with $_{HEa}$miRNA mimics significantly
290 reduced trophoblast invasion in the context of 320 mg/dL ethanol co-exposure, relative to the
291 control mimics (t(14)=2.762, p=0.015), consistent with our data demonstrating $_{HEa}$miRNAs
292 interfere with the EMT pathway (Figure 7A). Contrastingly, transfecting $_{HEa}$miRNA antagomirs

293 increased invasion in the context of 320 mg/dL ethanol co-exposure, though this effect was
294 only marginally significant (t(14)=1.805, p=0.093, Figure 7B).
295
296 $_{HEa}$miRNAs retard trophoblast cell cycle progression
297 Given the proliferative nature of cytotrophoblasts, and the intimate relationship
298 between EMT and cell cycle (72, 73), we assessed the effects of ethanol and $_{HEa}$miRNAs on
299 BeWO cytotrophoblast cell cycle. After pulse-labeling cells with the nucleic acid analog, EdU, for
300 1-hour, we found that individually transfecting 6 of the $_{HEa}$miRNA mimics increased EdU
301 incorporation (Unpaired t-test, $p<0.05$, FDR correction), suggesting an overall increased rate of
302 DNA synthesis (Supplementary Figure 7A). Contrastingly, simultaneous transfection of
303 $_{HEa}$miRNAs significantly reduced EdU incorporation($F_{(1,26)}=59.69$, $p<0.0001$), mirroring the
304 effects of increasing concentrations of ethanol ($R^2=0.304$, p=0.012) (Supplementary Figure 7B
305 and Figure 8A).
306 Consistent with the increased rates of DNA synthesis resulting from individual $_{HEa}$miRNA
307 mimic transfection, individual transfection of $_{HEa}$miRNAs antagomirs generally reduced EdU
308 incorporation, though only the antagomir to hsa-miR-760 did so significantly (t(110)=3.059,
309 p=0.003, FDR correction) (Supplementary Figure 7A). Interestingly, simultaneous administration
310 of antagomirs also reduced EdU incorporation, as observed with the pooled $_{HEa}$miRNAs mimics
311 ($F_{(1,26)}=34.83$, p=0.0005, Figure 8B).
312 To further characterize the coordinated effect of $_{HEa}$miRNAs on cytotrophoblast cell
313 cycle, we pulse-labeled cells with EdU for 1-hour and, post-fixation, labelled them with 7AAD to
314 segregate cells into three groups: G_0/G_1 (7AADlow, EDU-), S (EDU+), and G_2/M (7AADhigh, EDU-

315). Both 120 mg/dL and 320 mg/dL ethanol exposures significantly decreased the proportion of
316 cells in S-phase, while 320 mg/dL exposure increased the proportion of cells in G_2/M-phase,
317 consistent with the observed reduction in the rate of DNA synthesis (Supplementary Figure 7C).
318 Similar, to the effects of ethanol exposure, pooled $_{HEa}$miRNA mimic administration also
319 significantly decreased the proportion of cells in S-phase ($F_{(1,28)}$=52.78, p<0.0001) while
320 increasing the proportion of cells the G_2/M-phase ($F_{(1,28)}$=8.395, p=0.007) and exacerbated
321 alcohol's effects on the cell cycle (Figure 8C). Interestingly, pooled $_{HEa}$miRNA antagomir
322 administration also reduced the proportion of cells in S-phase ($F_{(1,26)}$=14.98, p=0.0007) and
323 increased the proportion of those in G_2/M-phase ($F_{(1,26)}$=12.38, p=0.002) (Figure 8D).
324 We sought to determine if pretreating cytotrophoblasts with pooled $_{HEa}$miRNA
325 antagomirs could prevent the cytotrophoblast cell cycle retardation caused by transfecting
326 $_{HEa}$miRNA mimics. Cells transfected with the control or pooled $_{HEa}$miRNA antagomirs, and
327 subsequently transfected with pooled $_{HEa}$miRNA mimics, did not have significantly different cell
328 cycle profiles or rates of DNA synthesis to each other but had significantly lower rates of DNA
329 synthesis (ANOVA, $F_{(2,12)}$=16.56, p=0.0004), and a decreased proportion of S-phase cells
330 ($F_{(2,12)}$=11.43, p=0.002) with an increased proportion of cells in G_2/M phase ($F_{(2,12)}$=11.47,
331 p=0.002), compared to cells transfected with both the control antagomir and control mimic
332 (Figures 9A and B). Collectively, our data indicate that transfection of these antagomirs
333 prevents further reduction in the rate of DNA synthesis, or cell cycle retardation, that would
334 result from transfection with pooled $_{HEa}$miRNA mimics.
335
336 <u>$_{HEa}$miRNAs have minimal effect on cell survival</u>

337 We next sought to investigate whether ethanol- and $_{HEa}$miRNA-induced changes in cell
338 cycle were related to an increase in cell death. Only the 320 mg/dL dose of ethanol exposure
339 demonstrated a slight, but marginally significant effect, of increasing lytic cell death
340 ($t(18)=2.022$, $p=0.054$), though there was no effect on apoptosis (Supplementary Figures 8A and
341 B). However, the changes in cell cycle following transfection of individual or pooled $_{HEa}$miRNA
342 mimics were not mirrored by changes in lytic cell death. Nevertheless, two $_{HEa}$miRNAs, hsa-mir-
343 671-5p and hsa-mir-449a, did significantly increase apoptosis (Unpaired t-test, $p<0.05$, FDR
344 correction) (Supplementary Figures 8C and D).
345 Contrastingly, transfection of 4 $_{HEa}$miRNA antagomirs individually, significantly increased
346 lytic cell death (Unpaired t-test, all $p<0.05$, FDR correction), with the antagomir to hsa-mir-491-
347 3p also increasing apoptotic cell death ($t(14)=3.383$, $p=0.004$, FDR correction, Supplementary
348 Figure 8C and D). Likewise, transfection of pooled $_{HEa}$miRNA antagomirs increased lytic cell
349 death ($F_{(1,36)}=11.40$, $p=0.002$) but did not cause increased apoptosis (Supplementary Figure 8E-
350 H). Taken together, our data suggest that while ethanol exposure may increase cytotrophoblast
351 death, increased levels of $_{HEa}$miRNAs have minimal effects on cell death, suggesting that their
352 effect on cell cycle and the EMT pathway is independent of any effect on cell survival.
353
354 <u>$_{HEa}$miRNAs modulate cytotrophoblast differentiation-associated Ca^{2+} dynamics</u>
355 $_{HEa}$miRNAs' effects on EMT pathway member expression, coupled with cell cycle
356 retardation, indicates that $_{HEa}$miRNAs influence trophoblast maturation. Maturation of
357 cytotrophoblasts into syncytiotrophoblasts is marked by dramatic changes in the cellular
358 energetics profile (74). To model $_{HEa}$miRNAs' effect on hormone-producing

359 syncytiotrophoblasts, we used a well-established protocol of forskolin induced syncytialization
360 of BeWO cytotrophoblasts (75, 76). As expected, forskolin treatment induced
361 fusion/syncytialization of cytotrophoblasts resulting in a greater average cell size in the
362 forskolin + $_{HEa}$miRNA mimics group ($F_{(1,386)}$=4.386, p=0.037). This suggests that the inhibition of
363 EMT by these miRNAs may result in preferential syncytialization instead of differentiation to
364 extravillous trophoblasts (Supplementary Figure 9A). Ethanol and forskolin treatment both
365 increased baseline calcium levels, as indicated by the change in fluo-4 fluorescence
366 ($F_{(1,426)}$=5.593 and 3.665 respectively, p<0.0001, Figure 10A, Supplementary Figures 9B-D). The
367 effect of ethanol on baseline calcium was abrogated by $_{HEa}$miRNAs while $_{HEa}$miRNAs + forskolin
368 was not significantly different to forskolin alone, indicating that forskolin and $_{HEa}$miRNAs may be
369 affecting similar calcium pathways. Syncytiotrophoblasts actively transport high amounts of
370 calcium from maternal to fetal circulation, therefore forskolin-exposed trophoblasts likely have
371 higher basal transport of calcium into the cells due to increased expression of plasma
372 membrane channels (77). The conversion of trophoblasts to synciotrophoblasts is accompanied
373 by an increase in endoplasmic reticulum, which could increase calcium buffering capabilities in
374 response to ethanol-stress on the cells, thus $_{HEa}$miRNA-induced syncytialization pathways may
375 be protective against ethanol stress.
376 Adaptations to cellular stress can be seen in alterations to cellular energetics in
377 response to ethanol, as ethanol-exposed BeWO cells showed decreased baseline and stressed
378 oxygen consumption rates (OCR) ($F_{(1,28)}$=15.55 and 16.91, p=0.0005 and 0.0003 respectively)
379 and increased extracellular acidification rates (ECAR) ($F_{(1,28)}$=4.868, p=0.036). However,
380 $_{HEa}$miRNAs had minimal effects on metabolic activity (Figures 10D-10G).

381 Extracellular ATP has been shown to inhibit trophoblast migration (78) and can directly
382 stimulate increased intracellular calcium elevations through purinergic receptors ubiquitously
383 present on trophoblasts (79). Both $_{HEa}$miRNA and ethanol administration significantly increased
384 intracellular calcium in response to acute ATP administration ($F_{(1,426)}$=10.34 and $F_{(1,386)}$=16.30,
385 p=0.001 and p<0.0001 respectively) (Figure 10B). This may be indicative of a lack of
386 downregulation of purinergic receptors required in trophoblast migration as part of the
387 interrupted EMT pathway. Forskolin-induced maturation decreased calcium response to ATP
388 ($F_{(1,386)}$=50.72, p<0.0001) (Figure 10C) and prevented the $_{HEa}$miRNA-induced increase in ATP
389 response. These data agree with previous studies showing increased nuclear trafficking of
390 ionotropic receptor P2X7 and more localized P2X4 expression over placental development,
391 which may decrease the overall calcium influx in response to ATP (80).
392
393 <u>$_{HEa}$miRNAs promotes syncytialization-dependent hormone production</u>
394 Transfection of $_{HEa}$miRNA mimics did not change *CGA*, *CGB*, or *IGF2* transcript expression
395 relative to the control in non-syncytialized trophoblasts. However, following syncytialization,
396 $_{HEa}$miRNA mimics significantly increased expression of *CGA* and *CGB* (post-hoc Tukey's HSD,
397 n=10 samples per group, p=0.001 and 0.005 respectively). Consistent with our previous results,
398 $_{HEa}$miRNA mimics also increased *CDH1* expression in both cytotrophoblasts and
399 syncytiotrophoblasts ($F_{(1,20)}$=5.286, p=0.032); there was also a main effect of syncytialization on
400 *CDH1* expression, as has been previously reported ($F_{(1,36)}$=3.391, p=0.034, Figures 11A-D).
401 Likewise, $_{HEa}$miRNAs increased E-cadherin protein expression ($F_{(1,20)}$=5.286, p=0.032), whereas
402 forskolin decreased it ($F_{(1,20)}$=10.24, p=0.005) (Figure 11E). On the other hand, there was no

403 effect of $_{HEa}$miRNA antagomirs on *CGA* and *CGB* expression, although we did observe a decrease
404 in *IGF2* transcript expression, following syncytialization, relative to controls (post-hoc Tukey's
405 HSD, n=10 samples per group, p=0.001) (Figure 11F-I).

406 Given that $_{HEa}$miRNAs promotes syncytialization-dependent hormone production, we
407 next investigated maternal plasma levels of intact human chorionic gonadotropin (hCG) in our
408 Ukraine birth cohort. Plasma hCG levels were non-significantly increased in the second
409 trimester of HEa group mothers relative to their UE counterparts, consistent with previous
410 studies (81). During the third trimester, however, hCG levels remained significantly elevated in
411 HEa group mothers compared to the UE group (Median Test, n=23 samples in HEa group and
412 n=22 for HEua and HEa groups, p=0.03) (Figure 12). Furthermore, there was no significant
413 difference of gestational age at blood draw between the different groups indicating the
414 increased level of hCG in the HEa group was not confounded by gestational age at which blood
415 was sampled (Supplementary Figure 10) (82). Interestingly, both alcohol and hCG levels were
416 negatively associated with gestational age at delivery (GAD), with a significant interaction
417 between periconceptional alcohol exposure and hCG levels on GAD (Supplementary Table 3).
418 Taken together, our data suggests $_{HEa}$miRNAs may contribute to PAE-dependent increases in
419 hCG levels during pregnancy.

420

421 <u>$_{HEa}$miRNAs reduce fetal growth</u>

422 To investigate the functional consequences of elevated circulating $_{HEa}$miRNA levels, we
423 administered miRNA mimics for the 8-mouse homologue $_{HEa}$miRNAs, or a negative control
424 mimic, through tail-vein injection to pregnant mouse dams on GD10. On GD18, growth

425 parameters of male and female fetuses were assessed separately, and data from all same-sex
426 fetuses from a single pregnancy were averaged into one data point. Dams administered
427 $_{HEa}$miRNA mimics produced smaller fetuses than those administered control mimics, according
428 to all collected measures of fetal size: fetal weight ($F_{(1,17)}$=9.92, p=0.006), crown-rump length
429 ($F_{(1,17)}$=9.89, p=0.006), snout-occipital distance ($F_{(1,17)}$=9.09, p=0.008), and biparietal diameter
430 ($F_{(1,17)}$=5.99, p=0.026) (Figure 13B-E). Interestingly, placental weights were also significantly
431 reduced in mice treated with $_{HEa}$miRNA mimics ($F_{(1,17)}$=6.92, p=0.018) (Figure 13F).

432 Following tail-vein administration of two human-specific sentinel miRNAs, miR-518f-3p
433 and miR-519a-3p, we found a high biodistribution of both miRNAs in the placenta, comparable
434 to levels seen in the liver and spleen (Supplementary Figure 11A and 10B). Thus, to determine
435 whether $_{HEa}$miRNA's effects on fetal growth could result from their actions on the placenta, we
436 quantified the placental expression of core EMT members in the GD18 placentas of control and
437 $_{HEa}$miRNA fetuses. $_{HEa}$miRNA administration significantly reduced expression of mesenchymal-
438 associated transcript *VIM* ($F_{(1,14)}$=14.23, p=0.002) and S*NAI2* ($F_{(1,14)}$=5.99, p=0.028) with a
439 significant sex by $_{HEa}$miRNA interaction effect on *SNAI1* ($F_{(1,66)}$=5.55, p=0.034) and *CDH1*
440 ($F_{(1,14)}$=6.01, p=0.028) (Figures 14A-E). Interestingly, and in line with our in vitro findings
441 whereby $_{HEa}$miRNAs promoted syncytialization dependent cell fusion and hCG production,
442 $_{HEa}$miRNA administration significantly increased expression of the mRNA transcript for *SynB*, a
443 gene that is important for syncytiotrophoblast maturation ($F_{(1,66)}$=4.11, p=0.047) (Figure 14F).

444 **Discussion**

445 In a prior study, we reported that gestational elevation of 11 maternal plasma miRNAs,
446 in a Ukrainian clinical cohort, predicted which PAE infants would exhibit adverse outcomes at
447 birth (11). These $_{HEa}$miRNAs were elevated throughout mid and late-pregnancy, encompassing
448 critical periods for fetal development, and were predicted to target key developmental
449 pathways (11). Given that $_{HEa}$miRNAs are placentally enriched and their dysregulation is
450 associated with placental-associated gestational pathologies, we sought to determine if they
451 also contributed to the pathophysiology of FASDs.

452 To mimic the alcohol consumption patterns in our Ukrainian cohort, we adopted
453 moderate alcohol self-administration paradigms during mouse and macaque gestation. Though
454 these species share a hemochorial placenta, fundamental differences in placental anatomy
455 remain. Specifically, macaque trophoblasts exhibit deeper invasion into the uterine horn than
456 their mouse counterparts (83-86). Despite these differences, we found PAE inhibited
457 mesenchymal transition-associated mRNA transcripts in both our models, indicating a
458 conserved effect of PAE on placental development. Additionally, we found that $_{HEa}$miRNAs
459 mediated the effects of PAE on core EMT pathway members in the placenta, and collectively
460 though not individually, inhibited EMT in human cytotrophoblast and extravillous trophoblast
461 culture models. The components of the EMT pathway were selected for assessment based on a
462 substantial literature that implicates these as core EMT components (13, 17, 18, 67-70).
463 However, analysis of their 3'UTRs indicates that these are unlikely to be the direct targets of
464 $_{HEa}$miRNA action. Additional studies will be needed to dissect out the signaling networks that
465 connect $_{HEa}$miRNAs to the assessed EMT components.

466 Interestingly, $_{HEa}$miRNAs also promoted syncytialization (forskolin)-dependent hCG
467 expression, mirroring the elevation of third trimester maternal hCG levels in the PAE group
468 within our Ukrainian birth cohort. This late-gestation elevation of hCG levels may serve as a
469 compensatory mechanism to prevent the preterm birth associated with PAE, as hCG during late
470 gestation is hypothesized to promote uterine myometrial quiescence (87, 88). In support of this
471 hypothesis, we found significant negative associations between both hCG levels and alcohol
472 consumption with gestational age at delivery. Furthermore, there was a significant interaction
473 between periconceptional alcohol exposure and hCG levels, with higher hCG levels
474 corresponding to a smaller effect of alcohol exposure at conception on gestational age at
475 delivery, indicating that hCG moderates the effect of alcohol on age at delivery (Supplementary
476 Table 3).
477 Since $_{HEa}$miRNAs collectively prevented trophoblast EMT, we hypothesized that, as a
478 functional consequence, these maternal miRNAs would also inhibit fetal growth. When we
479 delivered 8 out of the 11 $_{HEa}$miRNAs known to be present in mouse, to pregnant dams during
480 the period of placental branching morphogenesis and endometrial invasion , when EMT is
481 particularly active, we found that $_{HEa}$miRNAs reduced fetal growth. Importantly, ethanol
482 exposure during this period has also been shown to result in fetal growth deficits and
483 dysmorphia in rodent PAE models (89, 90) suggesting that maternal miRNA-mediated deficits in
484 trophoblast invasion may mediate some of the effects of PAE on fetal growth. In support of this,
485 we found placentas from the $_{HEa}$miRNA treated group had impaired expression of core EMT
486 pathway members. It is also feasible that $_{HEa}$miRNAs disrupt fetal growth through placental
487 vascular dynamics. The non-human primate tissue analyzed here was derived from animals that

488 were characterized in vivo using MRI and ultrasound imaging, which demonstrated that
489 maternal blood supply to the placenta was lower in ethanol-exposed animals compared to
490 controls, and that oxygen availability to the fetal vasculature was reduced (91). Thus, one
491 possibility is that compromised trophoblast invasion contributes to impaired maternal blood
492 flow in ethanol-exposed individuals, as we have also previously observed in mouse models (92).
493 Impaired nutrient uptake in the placenta, such as dysfunction in the amino acid, glucose,
494 and fatty acid transport systems have also been implicated in gestational pathologies, such as
495 intrauterine growth restriction (93). Furthermore, *in vitro* studies in trophoblasts have shown
496 alcohol exposure selectively impairs a subset of these amino acid and fatty acid transport
497 systems (94, 95) whilst *in vivo*, PAE in rodents alters expression of glucose transporters in the
498 late gestation placenta (23). These placental dysfunctions could also have insidious effects on
499 development that are not immediately detectable at birth. As an example, perturbations in
500 placental iron transport by PAE may impair central nervous system development during the
501 neonatal period, leading to cognitive deficits that last throughout adulthood (96, 97). Thus,
502 further investigation is warranted to determine if $_{HEa}$miRNAs contribute to this alcohol induced
503 impairment in trans-placental nutrient transport, and ultimately whether this impairment of
504 nutrient transport represents another avenue through which PAE disrupts fetal development.
505 It is likely that $_{HEa}$miRNAs may mediate other pregnancy associated pathologies, aside
506 from PAE. We identified numerous studies that reported increased circulating and placental
507 levels of at least 8 out of 11 $_{HEa}$miRNAs in gestational pathologies arising from placental
508 dysfunction. For example, elevated levels of one $_{HEa}$miRNA, miR-519a-3p, a member of the
509 placentally-expressed C19MC family cluster, was reported in placentae of patients with pre-

510 eclampsia, recurrent spontaneous abortion, and intrauterine growth restriction (40, 41, 54, 55).
511 Interestingly, collective overexpression of the 59 C19MC miRNAs inhibits trophoblast migration,
512 explaining their enrichment in the non-migratory villous trophoblasts and suggests their
513 downregulation is necessary for maturation into invasive extravillous trophoblasts (98). Thus, a
514 greater understanding of the placental roles of $_{HEa}$miRNAs may also help disentangle the
515 etiology of other pregnancy complications.

516 While our data suggest that the placenta is an important contributory source for
517 circulating $_{HEa}$miRNAs, the effects of $_{HEa}$miRNAs likely extend beyond the placenta into other
518 maternal tissues. Outside of the placenta, $_{HEa}$miRNAs may circulate in association with
519 lipoprotein complexes, or be encapsulated in extracellular vesicles (EVs) whose abundance
520 dramatically increases during pregnancy (99, 100). Recent work has demonstrated that
521 placental-derived EVs can regulate the maternal immune system as well as confer viral
522 resistance to recipient cells, including endothelial cells (101-104). Interestingly, other studies
523 also have identified endothelial cells as ready recipients for placental-derived EVs, suggesting
524 placental-EVs and their cargo miRNAs participate in synchronizing the growth of the placenta
525 with the accompanying maternal and fetal vascular remodeling (99, 105). While further
526 investigation is warranted into the role of EVs and miRNAs in maternal-fetal communication,
527 and to the extent they serve as paracrine/endocrine mediators for the placenta during
528 development, targeting $_{HEa}$miRNAs will likely have profound effects for both fetal and placental
529 development in the context of FASDs and other gestational pathologies.

530 While we did not investigate the effects of PAE on EMT in non-placental organs, it is
531 likely that PAE broadly disrupts EMT in multiple fetal compartments. Developmental ethanol

532 exposure has been shown inhibit the EMT-dependent migration of neural crest progenitors
533 involved in craniofacial development, explaining the facial dysmorphology seen in FAS and
534 FASDs (106, 107). Outside of its effects on the neural crest, PAE is significantly associated with
535 various congenital heart defects, including both septal defects and valvular malformations (108-
536 111). Septation of the heart, primarily atrial septation, is an EMT-dependent process, with
537 endocardial cells delaminating and transdifferentiating into mesenchymal cells that populate
538 the endocardial cushions as well as the muscular cap, which functions as the growing edge of
539 the muscular atrial septum(112, 113). The mesenchymal cells from the endocardial cushions
540 also form the cardiac valve progenitors. Thus, disruption of endocardial EMT could explain both
541 the valvular and septal malformation associated with PAE.

542 Collectively, our data on $_{HEa}$miRNAs suggest miRNA-based interventions could minimize
543 or reverse developmental effects of PAE and other placental-related pathologies. miRNA-based
544 therapeutic approaches have been advanced for other disease conditions. For example,
545 Miraversen^{tm}, an anti-miR-122 antisense oligonucleotide, has been shown to be effective in
546 reducing hepatitis-C viral burden (114). Additionally, a recent phase-1 clinical trial report
547 indicated that liposomal delivery of a tumor-suppressor miRNA was well tolerated in human
548 populations and showed evidence of therapeutic efficacy (115). However, we also observed
549 with $_{HEa}$miRNAs that the effects of combinations of miRNAs are not a sum of their individual
550 effects. Functional synergy between clusters of co-regulated miRNAs may be a common feature
551 in development and disease. For instance, in 2007, we presented early evidence that ethanol
552 exposure reduced miR-335, -21, and -153 in neural progenitors and that coordinate reduction
553 in these miRNAs yielded net resistance to apoptosis following ethanol exposure (116). In that

554 study, we also showed that coordinate knockdown of these three miRNAs was required to
555 induce mRNA for Jagged-1, a ligand for the Notch cell signaling pathway, an outcome that was
556 not recapitulated by knocking down each miRNA individually (116). More recently, combined
557 administration of miR-21 and miR-146a has been shown to be more effective in preserving
558 cardiac function following myocardial infarction than administration of either of these miRNAs
559 alone (117). While miRNA synergy has not been explored in detail, these data show that new
560 biology may emerge with admixtures of miRNAs, and that therapeutic interventions may
561 require the use of such miRNA admixtures rather than single miRNA molecules as have been
562 used in clinical studies to date. Our study was restricted to exploring the effects of the 11
563 $_{HEa}$miRNAs on development, which represent only the significantly increased fraction of miRNAs
564 elevated in the HEa group maternal plasma within our Ukrainian cohort. Indeed, the next 5
565 most elevated miRNAs are also abundantly expressed in the placenta (data not shown),
566 indicating they may also mediate the effects of PAE on placental biology.

567 In conclusion, we have observed how a set of 11 miRNAs, predictive of adverse infant
568 outcomes following PAE, collectively mediate the effects of alcohol on the placenta. Specifically,
569 elevated levels of these miRNAs promote an aberrant maturational phenotype in trophoblasts
570 by inhibiting core members of the EMT pathway and promoting syncytialization-dependent
571 hormone production. Functionally, these miRNAs are clinically correlated with measures of
572 fetal development and directly cause intrauterine growth restriction when administered in vivo.
573 Our work suggests that a greater understanding for the role of $_{HEa}$miRNAs during development,
574 and their role in coordinating the EMT pathway in the placenta and other developing tissues,

575 will benefit the understanding of FASDs and other gestational pathologies and potentially lead

576 to effective avenues for intervention.

577 **Methods**

578 Mouse model of PAE:

579 C57/BL6J mice (Jackson Laboratory, Bar Habor, ME) were housed under reverse 12-hour dark /
580 12-hour light cycle (lights off at 08:00 hours). PAE was performed using a previously described
581 limited access paradigm of maternal drinking (118, 119). Briefly, 60-day old female mice were
582 subjected to a ramp-up period with 0.066% saccharin containing 0% ethanol (2 days), 5%
583 ethanol (2 days), and finally 10% ethanol for 4-hours daily from 10:00–14:00 beginning 2 weeks
584 prior to pregnancy, continuing through gestation (Supplementary Figure 2A). Female mice
585 offered 0.066% saccharin without ethanol during the same time-period throughout pregnancy
586 served as controls. Tissue from the labyrinth, junctional, and decidual zone of male and female
587 gestational day 14 (GD14) placentae were microdissected, snap-frozen in liquid nitrogen, and
588 stored at -80ºC preceding RNA and protein isolation.

589

590 Mouse model for $_{HEa}$miRNA overexpression:

591 For systemic administration of miRNAs, previously nulliparous C57/BL6NHsd dams (Envigo,
592 Houston, TX) were tail-vein-injected on GD10 with either 50 µg of miRNA miRVana^{TM} mimic
593 negative control (Thermo Fisher, Waltham, MA, Cat No. 4464061) or pooled $_{HEa}$miRNA
594 miRVana^{TM} mimics in In-vivo RNA-LANCEr II (Bioo Scientific, Austin, TX, 3410-01), according to
595 manufacturer instructions. The 50 µg of pooled $_{HEa}$miRNA mimics consisted of equimolar
596 quantities of mmu-miR-222-5p, mmu-miR-187-5p, mmu-mir-299a, mmu-miR-491-3p, miR-760-
597 3p, mmu-miR-671-3p, mmu-miR-449a-5p, and mmu-miR-204-5p mimics. For bio-distribution
598 studies, 50 µg of pooled equimolar quantities of hsa-miR-519a-3p and hsa-miR-518f-3p mimics were

599 injected via tail vein. These human miRNAs were selected because no mouse homologs are known to
600 exist and consequently, estimates for organ distribution of exogenous miRNAs in the mouse are unlikely
601 to be contaminated by the expression of endogenous murine miRNAs. GD10 is a time point near the
602 beginning of the developmental period of branching morphogenesis, immediately following
603 chorioallantoic attachment, during which the placenta invades the maternal endometrium
604 (120). At GD18, pregnancies were terminated with subsequent quantification of fetal weight,
605 crown-rump length, snout-occipital distance, biparietal diameter, and placental weight (Figure
606 13A). Subsequently, tissue was snap-frozen in liquid nitrogen, and stored at -80ºC preceding
607 RNA isolation.
608
609 Rat model of PAE:
610 Outbred nulliparous Sprague-Dawley rats were housed under a 12-hour light/12-hourdark
611 cycle. PAE in Sprague-Dawley was conducted according to our previously published exposure
612 paradigm (23, 121). Briefly, dams were given a liquid diet containing either 0% or 12.5% ethanol
613 (vol/vol) from 4 days prior to mating until GD4 (Supplementary Figure 2B). Dams had *ad libitum*
614 access to the liquid diet 21-hours daily and consumed equivalent calories. Water offered during
615 the remaining 3-hours of the day. On GD5, liquid diets were removed and replaced with
616 standard laboratory chow. On GD20, placentas were immediately separated into the labyrinth
617 and junctional zone, snap frozen in liquid nitrogen and stored at −80 °C preceding RNA
618 isolation.
619
620 Non-human primate model of PAE:

621 As previously described in detail (91), adult female rhesus macaques were trained to orally self-
622 administer either 1.5 g/kg/d of 4% ethanol solution (equivalent to 6 drinks/day), or an isocaloric
623 control fluid prior to time-mated breeding. Each pregnant animal continued ethanol exposure
624 until gestational day 60 (GD60, term gestation is 168 days in the rhesus macaque) (122).
625 Pregnancies were terminated by cesarean section delivery at three different time points; GD85,
626 GD110, or GD135 (Supplementary Figure 2C). The macaque placenta is typically bi-lobed with
627 the umbilical cord insertion in the primary lobe and bridging vessels supplying the fetal side
628 vasculature to the secondary lobe (Figure 2D showing gross placenta anatomy) (123) . Full
629 thickness tissue biopsies (maternal decidua to fetal membranes) were taken from both the
630 primary and secondary lobes of the placenta (Figure 2E showing H&E section of placenta).
631 Samples were immediately snap-frozen in liquid nitrogen and stored at -80°C preceding RNA
632 isolation.
633
634 <u>Cell culture trophoblast models:</u>
635 BeWO human cytotrophoblastic choriocarcinoma cells and HTR-8/SVneo extravillous cells were
636 sourced from ATCC (Manassas, VA, Cat No. CCL-98 and CRL-3271 respectively). BeWO cells
637 were maintained in HAM's F12 media containing penicillin (100 U/ml), streptomycin (100
638 µg/ml), and 10% vol/vol fetal calf serum (FCS) at 37°C and 5% CO_2. HTR8 cells were maintained
639 in RPMI-1640 media with 5% vol/vol FCS, under otherwise identical conditions. Culture medium
640 was replenished every 2 days and cells sub-cultured every 4-5 days.
641 BeWO cells were treated with 20 µm forskolin to induce syncytialization, as previously
642 described (124, 125). BeWO and HTR8 cells were also subjected to four separate ethanol

643 treatment conditions: 0 mg/dL, 60 mg/dl (13 mM),120 mg/dl (26 mM) or 320 mg/dl (70 mM).

644 To achieve HEamiRNA overexpression and inhibition, Dharmacon miRIDIAN™ miRNA mimics and

645 hairpin inhibitors [25 nM], or control mimic (Dharmacon, Lafeyette CO, Cat No. CN-001000-01-

646 05) and hairpin inhibitor (Dharmacon, Cat No. CN-001000-01-05) [25nm], were transfected into

647 subconfluent BeWO and HTR8 cells using RNAIMAX lipofection reagent (Thermo Fisher, Cat No.

648 13778).

649

650 Cell cycle analysis:

651 At 48-hours-post transfection, BeWO cells were pulsed with 10 µM EdU for 1-hour. Cells were

652 immediately harvested, and cell cycle analysis was performed with the Click-iT® EdU Alexa

653 Fluor® 488 Flow Cytometry Assay Kit (Thermo Fisher, Cat No. C10420), in conjunction with 7-

654 Amino-Actinomycin D (Thermo Fisher, Cat No. 00-6993-50), according to manufacturer

655 instructions, using the Beckman Coulter® Gallios 2/5/3 Flow Cytometer. Data was analyzed

656 using Kaluza software (Beckman Coulter, Brea, CA).

657

658 Cell death analysis:

659 BeWO cell culture was harvested 48-hours post transfection media was subjected to lactate

660 dehydrogenase (LDH) detection using the Pierce™ LDH Cytotoxicity Assay Kit (Thermo Fisher,

661 Cat No. 88953), according to manufacturer instructions, for lytic cell death quantification. The

662 Promega Caspase-Glo® 3/7 Assay Systems (Promega, Madison, WI, Cat No. G8091) was used to

663 quantify apoptotic cell death

664

665 Invasion assay:

666 At 24-hours post-transfection and/or ethanol exposure, HTR8 cells were serum starved for an
667 additional 18-hours. Subsequently, HTR8 cells were seeded onto trans-well permeable supports
668 precoated with 300 µg/mL Matrigel (Corning, Corning, NY, Cat No. 354248). After 24-hours,
669 cells remaining in the apical chamber were removed with a cotton swab. Cells that invaded into
670 the basal chamber were incubated with 1.2 mM 3-(4,5-dimethylthiazol-2-yl)-2,5-
671 diphenyltetrazolium bromide (MTT) for 3-hours, and the precipitate solubilized with 10% SDS in
672 0.01N HCl. Absorbance intensities were read at 570 nm in a Tecan Infinite® 200 plate reader.

673

674 Metabolic flux analysis and calcium imaging:

675 BeWO cells (10,000/well) were plated into Seahorse XF96 Cell Culture Microplates (Agilent
676 Biotechnology, Cat No. 103275-100). The oxygen consumption rate (OCR), a measure of
677 mitochondrial respiration, and extracellular acidification rate (ECAR), a measure of glycolysis,
678 were measured using the Seahorse XFe96 flux analyzer (Seahorse Bioscience, North Billerica,
679 MA). At the time of assay, cell culture medium was replaced with the appropriate pre-warmed
680 Seahorse XF Base Medium (Agilent Biotechnology, Santa Clara, CA, Cat No. 102353-100). OCR
681 and ECAR parameters were measured using the Seahorse XFp Cell Energy Phenotype Test Kit™
682 (Agilent Biotechnology, Cat No. 103275-100). Metabolic stress was induced by simultaneous
683 treatment with 1µm Oligomycin and 0.125µM Carbonyl cyanide p-[trifluoromethoxy]-phenyl-
684 hydrazone (FCCP).

685 BeWO cells were also plated onto glass coverslips in 24 well plates at a density of 30,000
686 cells/well. After exposure to ethanol and/or forskolin in culture, cells were prepared for calcium

687 imaging. After replacement of culture media with external imaging media (154 mM NaCl, 5 mM
688 KCl, 2 mM $CaCl_2$, 0.5 mM $MgCl_2$, 5 mM glucose, 10 mM HEPES, pH 7.4), cells were loaded for 35
689 minutes at 37°C with the calcium indicator dye fluo-4 AM (Thermo Fisher Scientific, Cat No.
690 F14201), at a final concentration of 5µM fluo-4 AM in 0.1% DMSO. After incubation, cells were
691 washed to remove remaining extracellular fluo-4 and imaged at 40x using confocal microscopy
692 (FV1200-equipped BX61WI microscope, Olympus Corporation, Center Valley, PA). Time-lapse
693 images were acquired at a frequency of 0.5Hz. Individual cells were manually outlined and area
694 and mean fluorescence intensity were obtained for each cell (FIJI image processing
695 package)(126) . To determine the functional calcium range of each cell, at the end of imaging,
696 cells were exposed to 5 µM ionomycin and 10 mM EGTA (0mM external Ca^{2+}, $F_{range} = F_{ionomycin}$-
697 F_{EGTA}). Baseline fluorescence was determined by averaging the lowest 5 consecutive
698 fluorescence values during the initial 5 minutes ($F_{baseline}$) which was then expressed as a
699 percentage of F_{range} ($\Delta F_{baseline} = (F_{baseline}-F_{EGTA})/F_{range}$ X100). Maximal intracellular calcium
700 response to 100 µM ATP was determined by averaging the highest 3 consecutive fluorescence
701 values during ATP application (F_{ATP}) and determining the amount of fluorescence as a
702 percentage of F_{range} ($\Delta F_{ATP} = (F_{ATP}-F_{EGTA})/F_{range}$ X100).
703
704 <u>Quantitative reverse transcriptase-polymerase chain reaction (qRT-PCR) analysis:</u>
705 Total RNA was extracted from tissue, well as BeWO and HTR8 cells, using the miRNeasy Mini kit
706 (Qiagen, Cat No. 217004). For miRNA qPCR assays, cDNA was synthesized from 200 ng of total
707 RNA using the miRCURY LNA Universal RT cDNA synthesis kit (Exiqon, Cat No. 203301/Qiagen,
708 Cat No. 339340, Germantown, MD) and expression was assessed using miRCURY LNA SYBR

709 Green (Exiqon, Cat No. 203401/Qiagen, Cat No. 339345). For mRNA qPCR assays, cDNA was
710 synthesized from 500 ng of total RNA using the qScript™ cDNA Synthesis Kit (Quanta/Qiagen,
711 Cat No. 95047). Gene expression analysis was performed using PerfeCTa SYBR Green FastMix
712 (Quanta, Cat No. 95073) on the ViiA 7 Real-Time PCR System (Thermo Fisher Scientific). The
713 data presented correspond to the mean $2^{-\Delta\Delta Ct}$ after being normalized to the geometric mean of
714 β-actin, Hypoxanthine-Guanine Phosphoribosyltransferase 1 (HPRT1), and 18s rRNA. Expression
715 data for miRNA was normalized to the geometric mean of miR-25-3p, miR-574-3p, miR-30b-5p,
716 miR-652-3p, and miR-15b-5p. For each primer pair, thermal stability curves were assessed for
717 evidence of a single amplicon and the length of each amplicon was verified using agarose gel
718 electrophoresis. A list of primers and their sequences is presented in Supplementary Table 1.
719
720 Western immunoblotting analysis:
721 Protein was extracted using 1X RIPA lysis buffer (Millipore Sigma, Burlington MA) supplemented
722 with Halt protease inhibitor cocktail (Thermo Fisher Scientific). Tissue was homogenized using
723 the Branson Sonifier 150. Protein concentration was determined using Pierce BCA protein assay
724 kit (Thermo Fisher Scientific) and 30 µg of protein was loaded onto a 4-12% Bis-Tris
725 (Invitrogen/Thermo Fisher Scientific, Cat No. NPO323BOX), size fractionated at 200 V for 35
726 minutes, and transferred to a PVDF membrane using the iBlot transfer system
727 (Invitrogen/Thermo Fisher Scientific). Blots with protein from cultured cells were blocked with
728 5% nonfat dry milk in tris-buffered saline containing Tween®-20 (TTBS) for 1-hour and
729 incubated overnight with primary antibody. The blot was then washed and incubated with an
730 HRP-conjugated goat anti-rabbit or anti-mouse IgG (Invitrogen) at dilution 1:1000 for 1-hour,

731 then developed using PerkinElmer Western Lightning Plus Chemi ECL (PerkinElmer; Waltham,
732 MA) and visualized using a CCD camera (Fluorchem Q, Alpha Innotech; San Leandro, CA). Blots
733 with protein from homogenized tissue were dried overnight, rehydrated in methanol, stained
734 with REVERT™ Total Protein Stain and developed with the Odyssey CLx Imaging System (LI-COR,
735 Lincoln, NE). Blots were then blocked with Odyssey® Blocking Buffer (TBS) for 1h and incubated
736 overnight with primary antibody. The blot was then washed and incubated with IRDye® 800CW
737 secondary antibody (LI-COR, Cat No. 925-32210). The following antibodies were used: β-Actin
738 HRP (Santa Cruz Biotechnology, Cat No. sc-47778); Goat anti-Mouse IgG (H+L) Secondary
739 Antibody, HRP (Thermo Fisher, Cat No. 62-6520); Goat anti-Rabbit IgG (H+L) Secondary
740 Antibody, HRP (Thermo Fisher, Cat No. 65-6120); purified Mouse Anti-E-Cadherin (BD
741 Biosciences, Cat No. 610181), Rabbit anti-vimentin antibody [EPR3776] (Abcam, Cat No. ab
742 924647). Protein levels were quantified using the densitometric analysis package in FIJI image
743 processing software (126).
744
745 ELISA:
746 The 2nd and 3rd trimester maternal plasma samples were collected as part of a longitudinal
747 cohort study conducted in two regions of Western Ukraine as part of the Collaborative Initiative
748 on Fetal Alcohol Spectrum Disorders (CIFASD.org) between the years 2006 and 2011, as
749 previously reported(11). Plasma, at a 1:1000 dilution, was subjected to hCG detection using
750 Abcam's intact human hCG ELISA kit (Cat no. ab100533) following the manufacturer's protocol.
751
752 Literature Review

753 We conducted a literature review for $_{HEa}$miRNAs and their associated gestational pathology
754 using the National Institute of Health's Pubmed search interface. For each miRNA, the following
755 search parameters were used:

756 *[miRX OR miR X OR miRNA X OR miRNAX or miRNX] AND MeSH Term*

757 where X represents the miRNA of interest and automatic term expansion was enabled. The
758 following MeSH terms, and related search terms (in brackets), were used: Fetal Growth
759 Retardation [Intrauterine Growth Retardation, IUGR Intrauterine Growth Restriction, Low Birth
760 Weight, LBW, Small For Gestational Age, SGA], Premature Birth [Preterm Birth, Preterm Birth,
761 Preterm Infant, Premature Infant, Preterm Labor, Premature Labor], Spontaneous Abortion
762 [Early Pregnancy Loss, Miscarriage, Abortion, Tubal Abortion, Aborted Fetus], Pre-Eclampsia
763 [Pre Eclampsia, Preeclampsia, Pregnancy Toxemia, Gestational Hypertension, Maternal
764 Hypertension], and Maternal Exposure [Environmental Exposure, Prenatal Exposure]. Returned
765 articles were subsequently assessed for relevance.

766

767 <u>Secondary analysis of RNA sequencing data:</u>

768 Expression levels of $_{HEa}$miRNAs in tissues were determined using the Human miRNA Expression
769 Database and the miRmine Human miRNA expression database(66, 127). For expression
770 analysis of $_{HEa}$miRNA pri-miRNAs, RNA sequencing data was used from NCBI's sequence read
771 archive (https://www.ncbi.nlm.nih.gov/sra). The accession numbers for the sequence files are:
772 uterus (SRR1957209), thyroid (SRR1957207), thymus (SRR1957206), stomach (SRR1957205),
773 spleen (SRR1957203), small intestine (SRR1957202), skeletal muscle (SRR1957201), salivary
774 gland (SRR1957200), placenta (SRR1957197), lung (SRR1957195), liver (SRR1957193), kidney

775 (SRR1957192), heart (SRR1957191), whole brain (SRR1957183), adrenal gland (SRR1957124),
776 bone marrow (ERR315396), colon (ERR315484), adipose tissue (ERR315332), and pancreas
777 (ERR315479). Deep sequencing analysis was conducted using the Galaxy version 15.07 user
778 interface according to the bioinformatics pipeline outlined in Supplementary Figure 1.
779
780 Statistical analyses:
781 Linear regression models were used to estimate associations between infant growth measures
782 and miRNA expression levels, gestational age at blood draw, the interaction between subject-
783 centered miRNA expression level and gestational age at blood draw, and child sex. Spearman
784 correlations between infant growth measures and subject-centered miRNA expression levels
785 were also calculated. Linear regression models were also used to estimate the associations
786 between gestational at birth and log-transformed hCG levels, ethanol intake, the interaction
787 between log-transformed hCG levels and ethanol intake, gestational at blood draw, and child
788 sex. Statistical Analysis and graphs were generated with GraphPad Prism 6 software (GraphPad
789 Software, Inc., La Jolla, CA), SPSS v24, or R version 3.3.1. Results are expressed as the mean ±
790 SEM, or alternatively as box-and-whisker plots with the bounds of the box demarcating limits of
791 1st and 3rd quartile, a median line in the center of the box, and whiskers representing the total
792 range of data. The overall group effect was analyzed for significance using 1-way MANOVA, 1-
793 way or 2-way ANOVA with Tukey's Honest Significance Difference (HSD) post-hoc testing when
794 appropriate (i.e. following a significant group effect in 1-way ANOVA or given a significant
795 interaction effect between experimental conditions in 2-way ANOVA), to correct for a family-
796 wise error rate. A 2-tailed Student's t-test was used for planned comparisons. For experiments

797 characterizing the individual effects of $_{HEa}$miRNAs against the control miRNA or antagomirs,
798 individual 2-tailed Student's t-test with 5% FDR correction was applied to account for multiple
799 comparisons. All statistical tests, sample-sizes, and post-hoc analysis are appropriately reported
800 in the results section. A value of $p < 0.05$ was considered statistically significant, and a value of
801 $0.1 < p < 0.05$ was considered marginally significant.
802
803 Study approval:
804 Human study protocols were approved by Institutional Review Boards at the Lviv National
805 Medical University, Ukraine, and the University of California San Diego as well as Texas A&M
806 University in the USA. Research was conducted according to the principles expressed in the
807 Declaration of Helsinki with written informed consent received from participants prior to
808 inclusion in the study. All rodent experiments were performed in accordance with protocols
809 approved by the University of New Mexico Institutional Animal Care and Use Committee
810 (IACUC), and the Texas A&M University IACUC. All procedures involving non-human primate
811 research subjects were approved by the IACUC of the Oregon National Primate Research Center
812 (ONPRC), and guidelines for humane animal care were followed. The ONPRC abides by the
813 Animal Welfare Act and Regulations enforced by the US Department of Agriculture.
814
815 Author contributions:
816 AT, RM and CC conceived of and planned the study. AT, AM, and NS designed and conducted
817 cell culture studies, and AT conducted in vivo, murine miRNA overexpression studies and
818 analyzed tissues from mouse, rat and primate PAE models. AA developed the mouse PAE model

819 and LA and KM developed the rat PAE model and provided tissues. VR, NN, CK and KG

820 developed the non-human primate model of PAE and provided RNA from microdissected

821 tissues. AW and CC performed statistical analyses of human studies. AT, AM and RCM

822 collaborated on all other statistical analyses. AT, AM, AW, NS, AA, VR, NN, CK, KG, CC, and RM

823 collaborated in preparing the manuscript.

824

825 **Table 1**

			Weight			Height			Head Circumference		
MIMAT #	miRNA	Trimester	Sig.	R^2	ρ	Sig.	R^2	ρ	Sig.	R^2	ρ
MIMAT0004569	hsa-miR-222-5p	2	0.821	1.224	-0.051	0.066	9.572	-0.179	0.8	1.732	-0.104
MIMAT0004561	hsa-miR-187-5p	2	0.462	6.347	0.068	0.17	12.607	-0.074	0.134	10.903	0.103
MIMAT0000687	hsa-mir-299-3p	2	0.552	1.113	0.029	0.069	9.299	-0.203	0.036*	8.65	0.1
MIMAT0004765	hsa-miR-491-3p	2	0.172	3.61	0.112	0.849	2.033	-0.055	0.024*	12.529	0.156
MIMAT0004948	hsa-miR-885-3p	2	0.142	4.227	-0.174	0.044*	7.667	-0.231	0.59	1.36	-0.115
MIMAT0002842	hsa-miR-518f-3p	2	0.246	2.517	0.134	0.918	2.134	-0.118	0.007**	14.561	0.219
MIMAT0004957	hsa-miR-760	2	0.059	6.314	0.195	0.22	4.096	0.079	0.055	10.158	0.195
MIMAT0003880	hsa-miR-671-5p	2	0.123	7.24	0.11	0.578	5.264	-0.031	0.073	10.794	0.107
MIMAT0001541	hsa-miR-449a	2	0.101	11.584	0.104	0.718	5.851	-0.072	0.173	10.036	0.068
MIMAT0000265	hsa-miR-204-5p	2	0.026*	12.377	0.184	0.272	4.973	0	0.131	7.095	0.108
MIMAT0002869	hsa-miR-519a-3p	2	0.034*	7.975	0.153	0.403	6.83	-0.012	0.093	8.181	0.096
MIMAT0004569	hsa-miR-222-5p	3	0.875	0.993	-0.046	0.018*	10.709	-0.196	0.577	4.696	-0.01
MIMAT0004561	hsa-miR-187-5p	3	0.538	2.055	0.049	0.37	2.029	-0.109	0.784	3.697	0.002
MIMAT0000687	hsa-mir-299-3p	3	0.511	0.762	0.005	0.514	1.769	-0.072	0.87	3.786	-0.077
MIMAT0004765	hsa-miR-491-3p	3	0.824	3.165	-0.028	0.2	12.122	-0.121	0.747	4.188	-0.081
MIMAT0004948	hsa-miR-885-3p	3	0.807	0.148	0.029	0.102	4.686	-0.156	0.376	5.009	0.032
MIMAT0002842	hsa-miR-518f-3p	3	0.515	2.099	0.109	0.421	1.715	0.016	0.245	7.917	0.152
MIMAT0004957	hsa-miR-760	3	0.368	1.396	0.141	0.761	0.716	-0.022	0.207	6.052	0.172
MIMAT0003880	hsa-miR-671-5p	3	0.055	8.715	0.155	0.367	3.521	-0.133	0.076	8.196	0.15
MIMAT0001541	hsa-miR-449a	3	0.995	0.085	-0.06	0.982	0.678	-0.151	0.026*	12.022	0.135
MIMAT0000265	hsa-miR-204-5p	3	0.019*	11.872	0.23	0.206	5.589	0.022	0.002**	18.683	0.319
MIMAT0002869	hsa-miR-519a-3p	3	0.391	2.82	0.043	0.302	5.917	-0.151	0.106	9.286	0.118

826

827 **Table 1: $_{HEa}$miRNAs are significantly correlated with independent measures of infant size**

828 The correlation of 2nd and 3rd trimester maternal plasma $_{HEa}$miRNA levels with independent
829 measures of infant size. $_{HEa}$miRNAs and their significantly correlated sex and gestational age-
830 adjusted growth parameters appear in red. *p<0.05, **p<0.01.

831

832 **Figures**

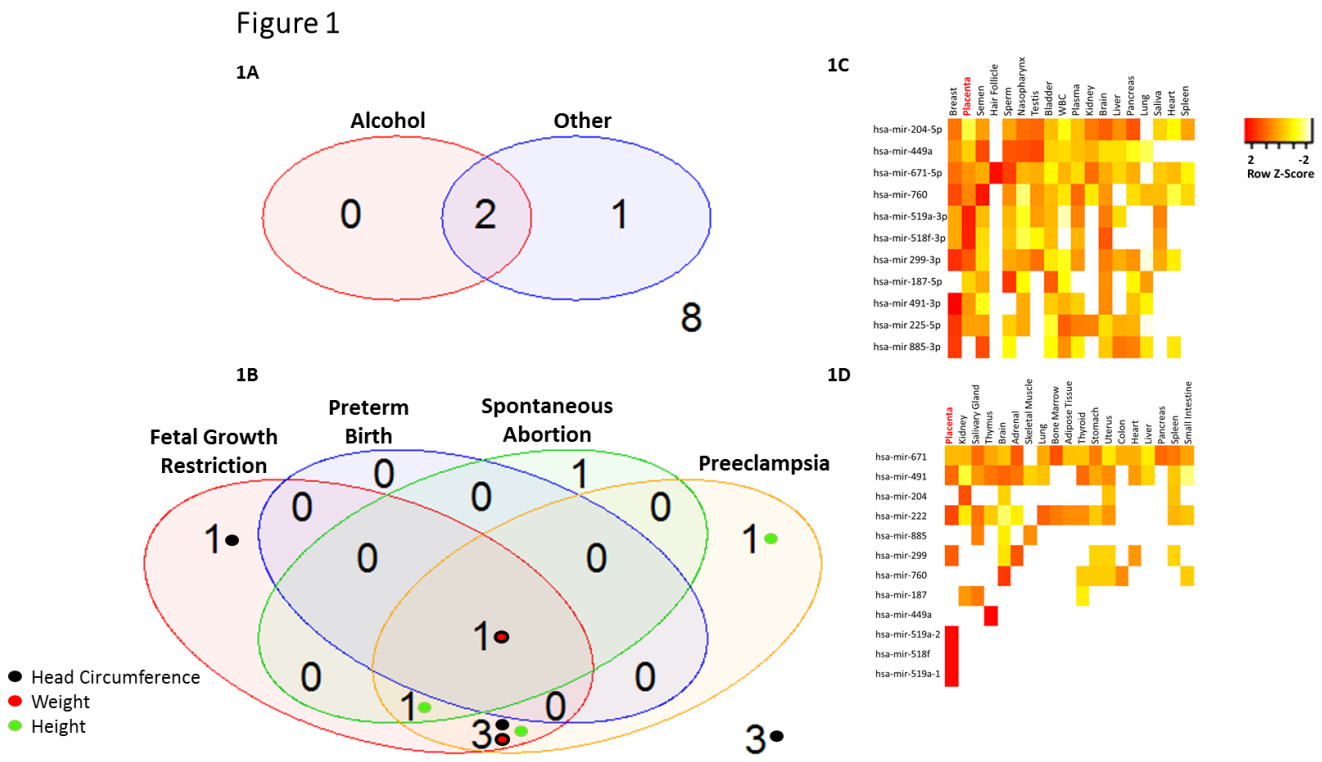

833

834 **Figure 1: $_{HEa}$miRNAs are placentally enriched and associated with gestational pathologies**

835 1A) Venn diagram on number of $_{HEa}$miRNAs reported to be associated with alcohol or other
836 prenatal exposures.

837 1B) Venn diagram on number of $_{HEa}$miRNAs reported to be associated with different gestational
838 pathologies. Inset colored circles represent the corresponding sex and gestational age-adjusted
839 growth parameters these miRNAs were correlated with. Of the 22 studies queried, 11 (50%)
840 utilized unbiased screenings for miRNA expression.

841 1C) Heatmap of mature $_{HEa}$miRNA expression and 1D) pri-$_{HEa}$miRNA expression across different
842 tissues resulting from secondary analysis of publicly available RNA-sequencing data. Legend
843 depicts row-centered Z-score.

844

Figure 2

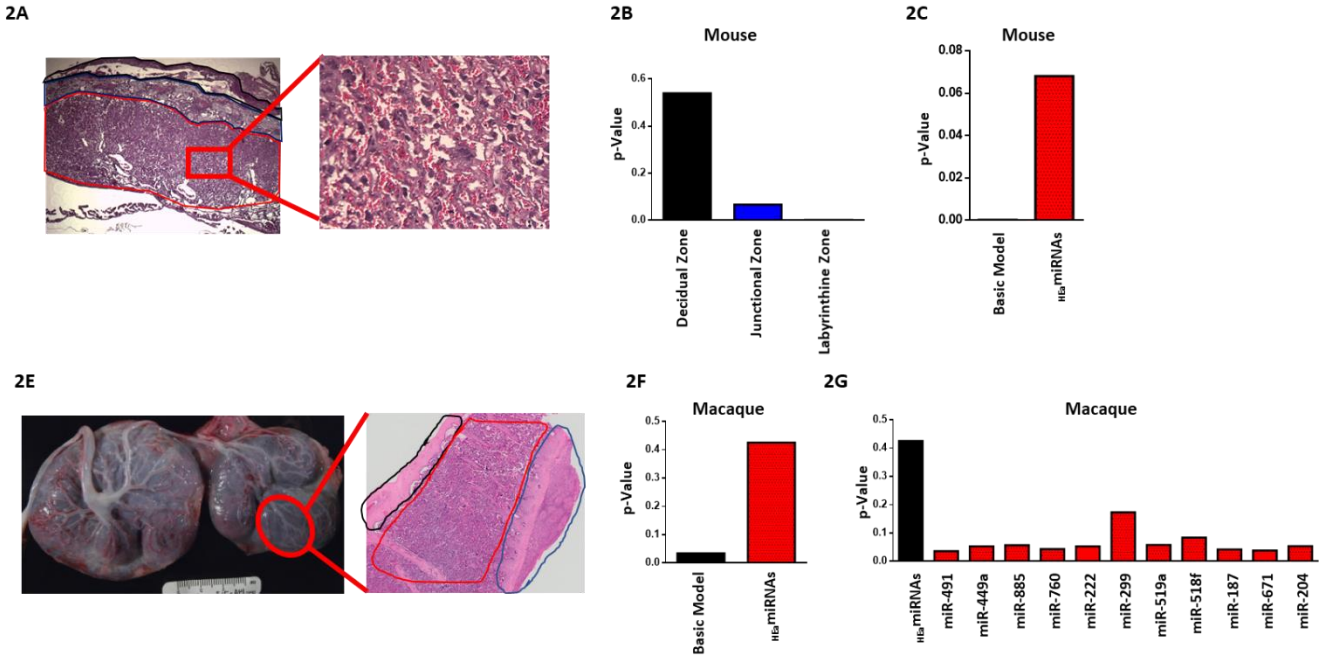

Figure 2: $_{HEa}$miRNAs mediate the effect of PAE on EMT pathway members in mouse and macaque placentas.

2A) Histological image of GD14 mouse placenta. Outlined in red is the labyrinth zone, blue is the junctional zone, black is the decidual zone. Inset is a high magnification image of the labyrinth zone.
2B) MANOVA of gene expression of core EMT pathway members in different regions of the mouse placenta in control and PAE mice (n=29 samples).
2C) MANCOVA of gene expression of core EMT pathway members in the mouse placental labyrinth zone before (Basic Model) and after accounting for the expression of $_{HEa}$miRNAs (n=29 samples).
2D) Gross anatomy photograph of the primary (left) and secondary (right) lobes of a GD135 macaque placenta. Outlined in red is an individual cotyledon from the secondary lobe. Inset is a full thickness hematoxylin and eosin stained histological section of a representative cotyledon with the fetal membranes outlined in black, villous tissue outlined in red and maternal decidua in blue.
2E) MANCOVA of gene expression of core EMT pathway members in placental cotyledons of PAE and control macaques, accounting for the expression of $_{HEa}$miRNAs collectively (n=23 samples).
2F) MANCOVA of gene expression of core EMT pathway members in macaque placentas after accounting for expression of $_{HEa}$miRNAs individually (n=23 samples).

Figure 3

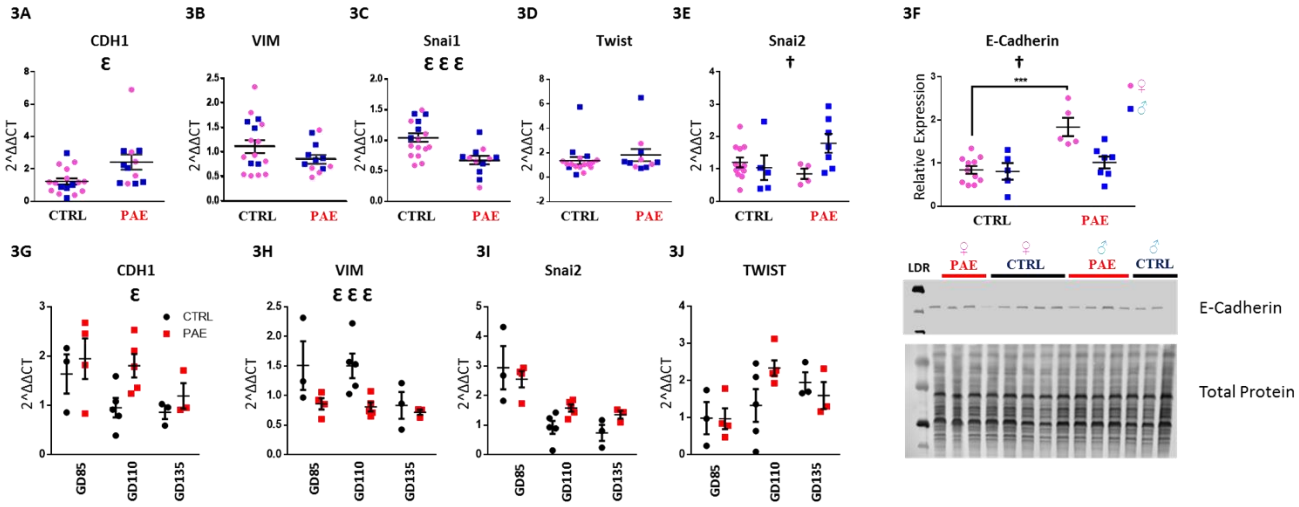

Figure 3: PAE interferes with EMT pathway member expression in mouse and macaque placentas

Expression of 3A) *CDH1*, 3B) *VIM*, 3C) *SNAI1*, 3D) *TWIST*, and 3E) *SNAI2* in the placental labyrinth zone of PAE and control mice (n=5-12 samples per group).

3F) Densitometric quantification of E-Cadherin expression in the labyrinth zone of PAE and control mice as well as representative blot of E-Cadherin expression (top) and total protein expression (bottom, n=5-12 samples per group).

Expression of 3G) *CDH1*, 3H) *VIM*, 3I) *SNAI2*, and 3J) *TWIST* transcripts in PAE and Control macaque placental cotyledons (n=3-5 samples per group).

Results are expressed as the mean ± SEM, LDR=Molecular Weight Ladder; ANOVA: significant main effect of PAE [$^{\varepsilon}p<0.05$, $^{\varepsilon\varepsilon\varepsilon}p<0.001$], significant interaction effect (sex by PAE, [$^{\dagger}p<0.05$]). For post-hoc analysis, ***p<0.001 by Tukey's HSD.

Figure 4

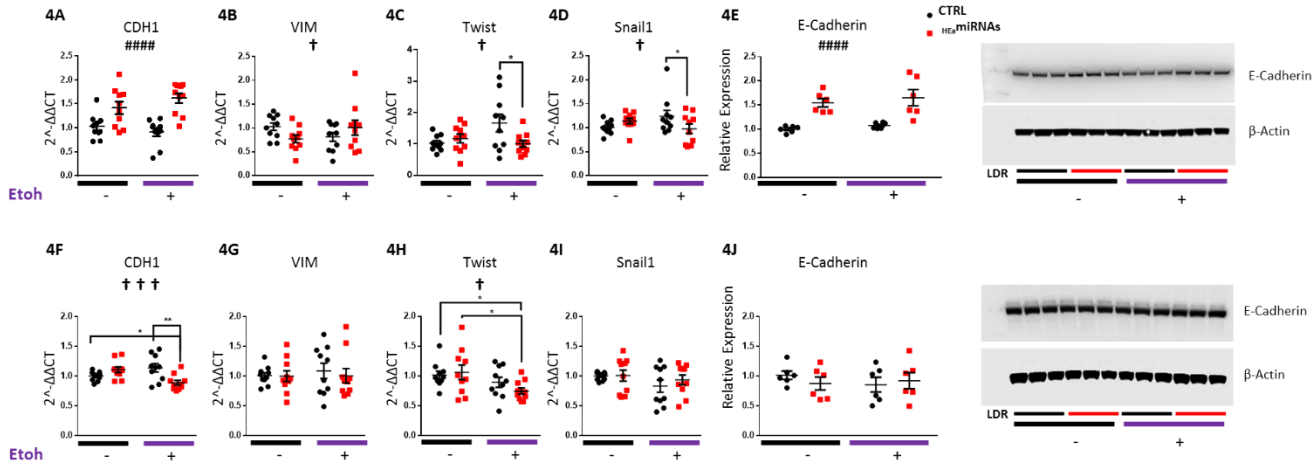

Figure 4: $_{HEa}$miRNAs interfere with EMT pathway member expression in BeWO cytotrophoblasts

Expression of 4A) *CDH1,* 4B) *VIM,* 4C) *TWIST,* and 4D) *SNAI1* transcripts 4E) and densitometric quantification of E-Cadherin protein levels in BeWO cytotrophoblasts following $_{HEa}$miRNAs or control miRNA overexpression with or without concomitant 320 mg/dL ethanol exposure.

4F) Expression of *CDH1,* 4G) *VIM,* 4H) *TWIST,* and 4I) *SNAI1* transcripts 4J) and densitometric quantification of E-Cadherin protein levels in BeWO cytotrophoblasts following $_{HEa}$miRNAs or control hairpin inhibitor transfection with or without concomitant 320 mg/dL ethanol exposure. Results are expressed as the mean ± SEM, LDR=Molecular Weight Ladder, n=10 samples per group; ANOVA: significant main effect of $_{HEa}$miRNA transfection [$^{\#\#\#\#}p<0.0001$], significant interaction effect ($_{HEa}$miRNA by 320mg/dL ethanol, [$^{\dagger}p<0.05$, $^{\dagger\dagger\dagger}p<0.001$]). For post-hoc analysis $^{*}p<0.05$, $^{**}p<0.01$ by Tukey's HSD.

Figure 5

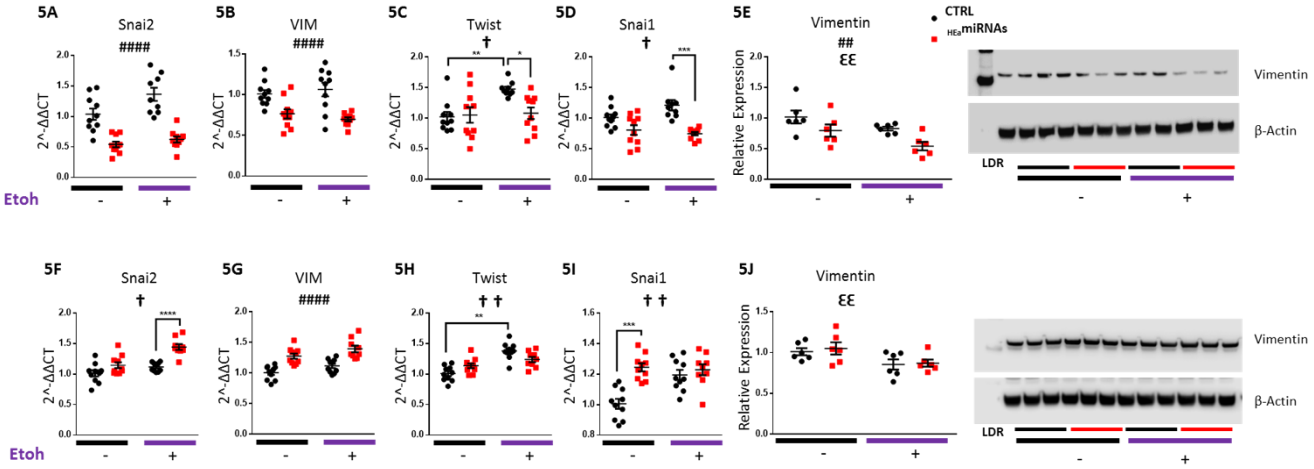

Figure 5: $_{HEa}$miRNAs interfere with EMT pathway member expression in HTR8 extravillous trophoblasts

Expression of 5A) *SNAI2* 5B) *VIM* 5C) *TWIST* and 5D) *SNAI1* transcripts 5E) as well as densitometric quantification of Vimentin protein levels in HTR8 extravillous trophoblasts following $_{HEa}$miRNAs or control miRNA overexpression with or without concomitant 320 mg/dL ethanol exposure.

Expression of 5F) *SNAI2* 5G) *VIM* 5H) *TWIST* and 5I) *SNAI1* transcripts 5J) as well as densitometric quantification of Vimentin protein levels in HTR8 extravillous trophoblasts following $_{HEa}$miRNA or control hairpin inhibitor transfection with or without concomitant 320 mg/dL ethanol exposure.

Results are expressed as the mean ± SEM, LDR=Molecular Weight Ladder, n=10 samples per group; ANOVA: significant main effect of $_{HEa}$miRNA transfection [$^{\#\#}$p<0.01, $^{\#\#\#\#}$p<0.0001], significant main effect of 320mg/dL ethanol exposure [^{ƐƐ}p<0.01], significant interaction effect ($_{HEa}$miRNA by 320mg/dL ethanol, [†p<0.05, ††p<0.01]). For post-hoc analysis *p<0.05, **p<0.01, ***p<0.001, and ***p<0.0001 by Tukey's HSD.

Figure 6

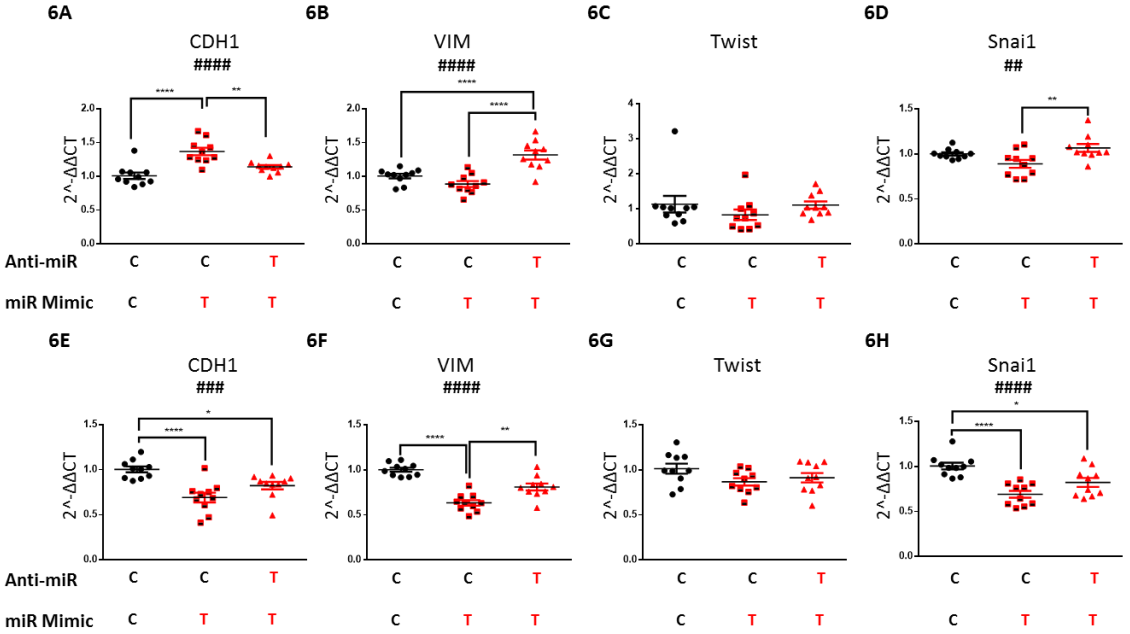

Figure 6: Antagomirs prevent $_{HEa}$miRNA induced impairment of EMT core pathway members

Expression of 6A) *CDH1* 6B) *VIM* 6C) *TWIST* and 6D) *SNAI1* Transcripts following control or $_{HEa}$miRNA hairpin inhibitor transfection followed by control or $_{HEa}$miRNA overexpression in BeWO cytotrophoblasts.

Expression of 6E) *CDH1* 6F) *VIM* 6G) *TWIST* and 6H) *SNAI1* Transcripts following control or $_{HEa}$miRNA antagomir transfection followed by control or $_{HEa}$miRNA overexpression in HTR8 extravillous trophoblasts.

In subheadings: **C** denotes control miRNA mimic or hairpin whereas **T** denotes $_{HEa}$miRNA mimic or hairpin inhibitor. Results are expressed as expressed as the mean ± SEM, n=10 samples per group; ANOVA: significant treatment effect [$^{##}$p<0.01, $^{###}$p<0.001, $^{####}$p<0.0001]. For post-hoc analysis, *p<0.05, **p<0.01, ***p<0.001, ****p<0.0001 by Tukey's HSD.

Figure 7

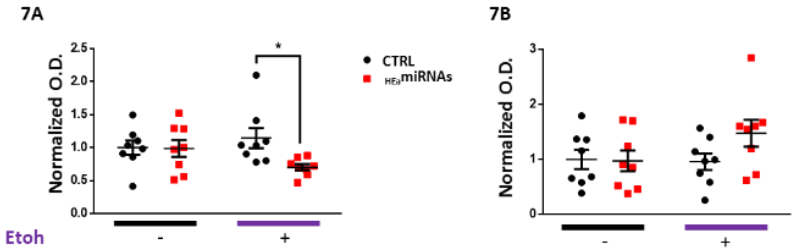

921
922 **Figure 7: $_{HEa}$miRNA impair extravillous trophoblast invasion**
923 Transwell invasion of HTR8 extravillous trophoblasts following transfection with 7A) $_{HEa}$miRNA
924 mimics or 7B) hairpin inhibitors with or without concomitant 320 mg/dL ethanol exposure.
925 Results are expressed as expressed as the mean ± SEM; n=10 samples per group; *p<0.05 by
926 Unpaired T-test
927

Figure 8

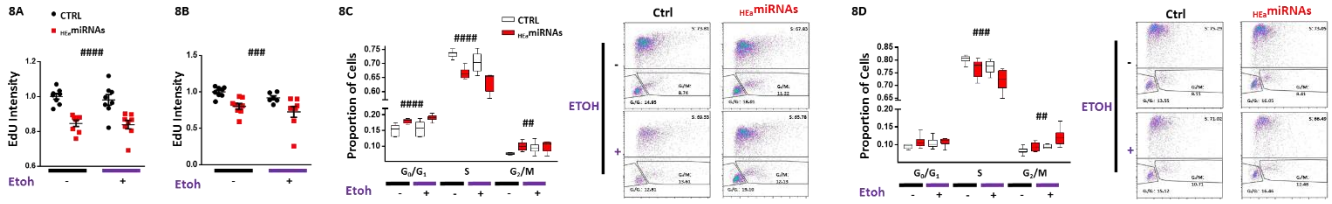

928

929 **Figure 8: $_{HEa}$miRNA cause cell cycle retardation in trophoblasts**

930 8A) Degree of EdU incorporation following control and $_{HEa}$miRNA overexpression or 8B) control
931 and $_{HEa}$miRNA hairpin inhibitor transfection with or without concomitant 320 mg/dL ethanol
932 exposure in BeWO cytotrophoblasts. Results are expressed as expressed as the mean ± SEM.
933 8C) Box and whisker plot for the proportion of cells in G_0/G_1, S, or G_2/M phase of the cell cycle
934 following control and $_{HEa}$miRNA overexpression or 8D) control and $_{HEa}$miRNA hairpin inhibitor
935 transfection with or without concomitant 320 mg/dL ethanol exposure. Bounds of box
936 demarcate limits of 1st and 3rd quartile, line in middle is the median, and whiskers represent
937 the range of data. Representative flow cytometry experiment images are shown on the right.
938 n=10 samples per group; ANOVA: significant main effect of $_{HEa}$miRNA transfection [$^{##}p<0.01$,
939 $^{###}p<0.001$, and $^{####}p<0.0001$].
940
941

Figure 9

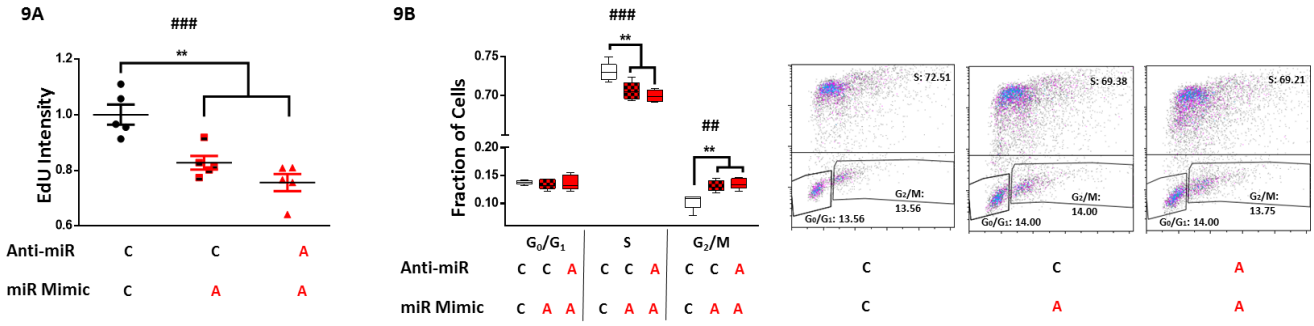

Figure 9: Antagomirs prevent $_{HEa}$miRNA induced cell cycle retardation

9A) Degree of EdU incorporation following control or $_{HEa}$miRNA hairpin inhibitor transfection followed by control or $_{HEa}$miRNA overexpression in BeWO cytotrophoblasts. Results are expressed as expressed as the mean ± SEM.

9B) Box and whisker plot for the proportion of cells in G_0/G_1, S, or G_2/M phase of the cell cycle following control or $_{HEa}$miRNA hairpin inhibitor transfection followed by control or $_{HEa}$miRNA overexpression in BeWO cytotrophoblasts. Bounds of box demarcate limits of 1st and 3rd quartile, line in middle is the median, and whiskers represent the range of data. Representative flow cytometry experiment images are shown on the right.

In subheadings: **C** denotes control miRNA mimic or hairpin whereas **T** denotes $_{HEa}$miRNA mimic or hairpin inhibitor. n=5 samples per group; ANOVA: significant treatment effect [$^{###}p<0.001$]. For post-hoc analysis, $^{**}p<0.01$ by Tukey's HSD.

Figure 10

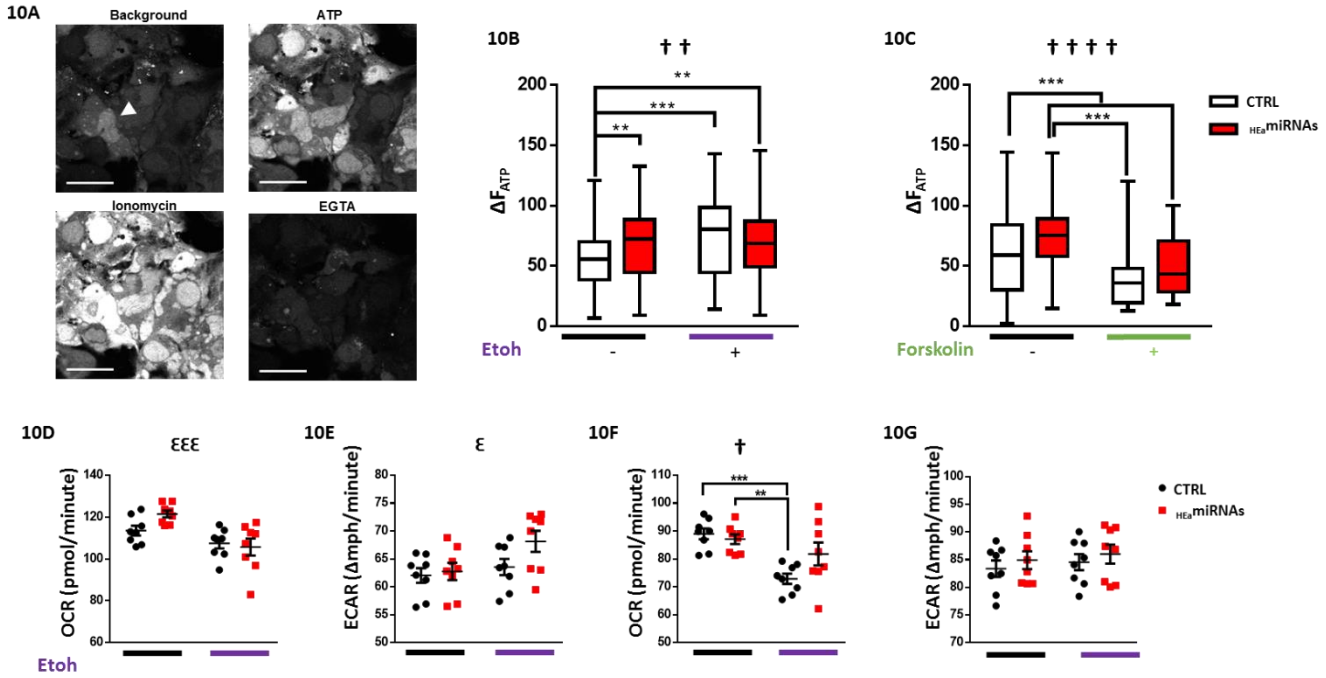

Figure 10: $_{HEa}$miRNAs modulate differentiation-associated Ca^{2+} dynamics but have minimal effect on the cellular energetics profile

10A) Time-lapse confocal images of BeWO cytotrophoblasts loaded with fluo-4 Ca^{2+} indicator dye under indicated treatment conditions. Arrowhead indicates a fused, multinuclear cell, scale bar is 50µm.

10B) Box and whisker plot of intracellular calcium levels following acute ATP administration in BeWO cytotrophoblasts with control and $_{HEa}$miRNA overexpression with or without concomitant 320 mg/dL ethanol exposure. Bounds of box demarcate limits of 1st and 3rd quartile, line in middle is the median, and whiskers represent the range of data.

10C) Box and whisker plot of intracellular calcium levels following acute ATP administration in BeWO cytotrophoblasts with control and $_{HEa}$miRNA overexpression with or without 20 µm forskolin treatment.

10D) Baseline oxygen consumption rate (OCR), 10E) baseline extracellular acidification rate (ECAR), 10F) stressed OCR, and 10G) stressed ECAR in BeWO cytotrophoblasts with control and $_{HEa}$miRNA overexpression with or without concomitant 320mg/dL ethanol exposure. Metabolic stress was induced by treatment with 1µm Oligomycin and 0.125µM (FCCP). Results are expressed as expressed as the mean ± SEM.

n=10 samples per group; ANOVA: significant main effect of 320mg/dL ethanol exposure [$^{\varepsilon}p<0.05$, $^{\varepsilon\varepsilon\varepsilon}p<0.001$], significant interaction effect ($_{HEa}$miRNA by 320mg/dL ethanol, [$^{\dagger}p<0.05$, $^{\dagger\dagger}p<0.01$, and $^{\dagger\dagger\dagger\dagger}p<0.0001$]). For post-hoc analysis, *p<0.05, **p<0.01, ***p<0.001, and ***p<0.0001 by Tukey's HSD.

Figure 11

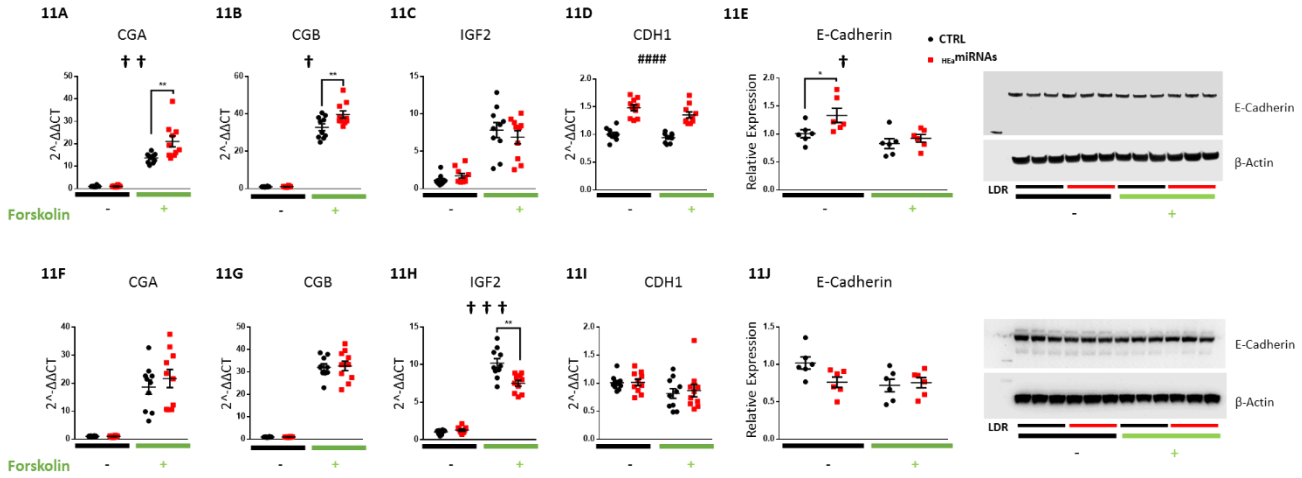

Figure 11: HEamiRNAs promote syncytialization dependent hCG production
Expression of 11A) *CGA,* 11B) *CGB,* 11C) *IGF2,* and 11D) *CDH1* transcripts 11E) and densitometric quantification of E-Cadherin protein levels in BeWO cytotrophoblasts following HEamiRNAs or control miRNA overexpression with or without 20 µm forskolin treatment. Expression of 11F) *CGA*, 11G) *CGB*, 11H) *IGF2*, and 11I) *CDH1* transcripts 11J) and densitometric quantification of E-Cadherin protein levels in BeWO cytotrophoblasts following HEamiRNAs or control hairpin inhibitor transfection with or without 20 µm forskolin treatment. Results are expressed as expressed as the mean ± SEM, LDR=Molecular Weight Ladder, n=10 samples per group; ANOVA: significant main effect of HEamiRNA transfection [$^{\#\#\#\#}p<0.0001$], significant interaction effect (HEamiRNA by 320mg/dL ethanol, [$^{\dagger}p<0.05$]). For post-hoc analysis, $^{*}p<0.05$, $^{**}p<0.01$ by Tukey's HSD.

Figure 12

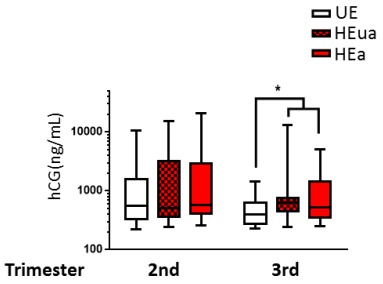

Figure 12: PAE elevates 3rd trimester maternal hCG

Box and whisker plot of 2nd and 3rd trimester maternal hCG levels in UE, HEua, and HEa group mothers of our Ukrainian birth cohort. Bounds of box demarcate limits of 1st and 3rd quartile, line in middle is the median, and whiskers represent the range of data. Results are expressed as expressed as the mean ± SEM, n=22-23 samples per group; *p=0.03 (Mood's Median Test, χ^2=7.043, df=2).

Figure 13

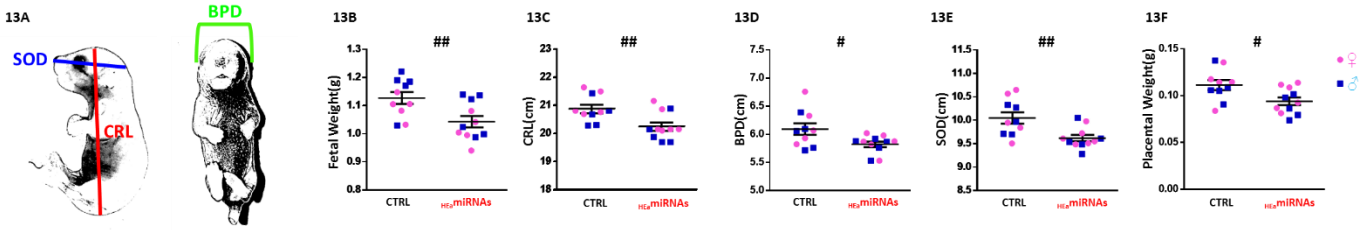

Figure 13: $_{HEa}$miRNAs restrict fetal growth

13A) Schematic for measures of crown rump length (CRL), biparietal diameter (BPD), and snout-occipital distance (SOD).

13B) Fetal weight, 13C) crown-rump length, 13D) biparietal diameter, 13E) snout-occipital distance, 13F) and placental weight at GD18 following administration of control (Ctrl) and $_{HEa}$miRNA mimics to pregnant C57/Bl6 dams on GD10. Dots represent median measures of fetal size and placental weights from male and female offspring in independent litters. There were no significant differences in litter sizes [Ctrl: 8.2 and $_{HEa}$miRNAs: 8.5] or sex ratios [Ctrl: 0.86 and $_{HEa}$miRNAs: 1.21] between treatment conditions ($p>0.5$ for all measures).

Results are expressed as expressed as the mean ± SEM, n=5-6 separate litters per treatment condition; ANOVA: significant main effect of $_{HEa}$miRNA administration [$^{\#}p<0.05$ and $^{\#\#}p<0.01$].

Figure 14

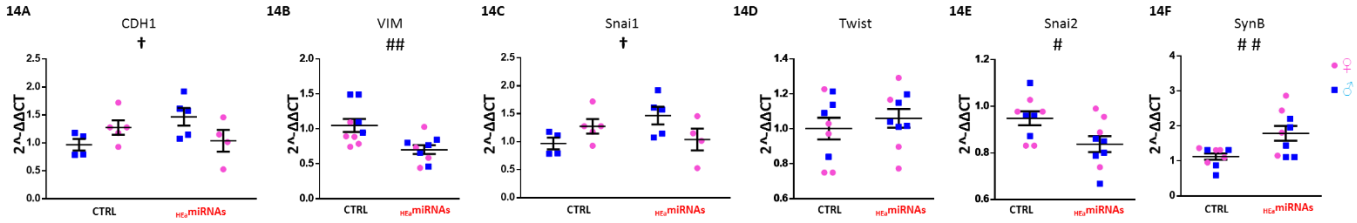

1017

1018 **Figure 14: $_{HEa}$miRNAs interfere with core EMT pathway members in the placenta**

1019 Expression of 14A) *CDH1* 14B) *VIM* 14C) *TWIST* 14D) *SNAI1* and 14E) *SynB* transcripts in
1020 GD18 placenta following administration of control (Ctrl) and $_{HEa}$miRNA mimics to pregnant
1021 C57/Bl6 dams on GD10.
1022 Dots represent median expression values of male and female offspring in independent litters.
1023 Results are expressed as expressed as the mean ± SEM, n=5-6 separate litters per treatment
1024 condition, ANOVA: significant main effect of $_{HEa}$miRNA administration [$^{\#}p<0.05$, $^{\#\#\#}p<0.001$],
1025 significant interaction effect (fetal sex by $_{HEa}$miRNA administration, [$^{\dagger}p<0.05$]). For post-hoc
1026 analysis, *p<0.05 by Tukey's HSD.

1027
1028
1029

1030 **References**

1031 1. ACOG. Committee opinion no. 496: At-risk drinking and alcohol dependence: obstetric and
1032 gynecologic implications. *Obstetrics and gynecology.* 2011;118(2 Pt 1):383-8.
1033 2. Popova S, Lange S, Probst C, Gmel G, and Rehm J. Estimation of national, regional, and global
1034 prevalence of alcohol use during pregnancy and fetal alcohol syndrome: a systematic review and
1035 meta-analysis. *The Lancet Global Health.* 2017;5(3):e290-e9.
1036 3. SAMHSA. The NSDUH Report: 18 percent of pregnant women drink alcohol during early
1037 pregnancy. *NSDUH Report.* 2013.
1038 4. Bakhireva LN, Sharkis J, Shrestha S, Miranda-Sohrabji TJ, Williams S, and Miranda RC. Prevalence
1039 of Prenatal Alcohol Exposure in the State of Texas as Assessed by Phosphatidylethanol in
1040 Newborn Dried Blood Spot Specimens. *Alcohol Clin Exp Res.* 2017;41(5):1004-11.
1041 5. Riley EP, Infante MA, and Warren KR. Fetal alcohol spectrum disorders: an overview.
1042 *Neuropsychol Rev.* 2011;21(2):73-80.
1043 6. May PA, Gossage JP, Kalberg WO, Robinson LK, Buckley D, Manning M, et al. Prevalence and
1044 epidemiologic characteristics of FASD from various research methods with an emphasis on
1045 recent in-school studies. *Developmental disabilities research reviews.* 2009;15(3):176-92.
1046 7. May PA, Blankenship J, Marais AS, Gossage JP, Kalberg WO, Barnard R, et al. Approaching the
1047 prevalence of the full spectrum of fetal alcohol spectrum disorders in a South African
1048 population-based study. *Alcohol Clin Exp Res.* 2013;37(5):818-30.
1049 8. Popova S, Lange S, Probst C, Gmel G, and Rehm J. Estimation of national, regional, and global
1050 prevalence of alcohol use during pregnancy and fetal alcohol syndrome: a systematic review and
1051 meta-analysis. *Lancet Glob Health.* 2017;5(3):e290-e9.
1052 9. Roozen S, Peters GJ, Kok G, Townend D, Nijhuis J, and Curfs L. Worldwide Prevalence of Fetal
1053 Alcohol Spectrum Disorders: A Systematic Literature Review Including Meta-Analysis. *Alcohol*
1054 *Clin Exp Res.* 2016;40(1):18-32.
1055 10. Popova S, Lange S, Burd L, and Rehm J. The Economic Burden of Fetal Alcohol Spectrum Disorder
1056 in Canada in 2013. *Alcohol and Alcoholism.* 2016;51(3):367-75.
1057 11. Balaraman S, Schafer JJ, Tseng AM, Wertelecki W, Yevtushok L, Zymak-Zakutnya N, et al. Plasma
1058 miRNA Profiles in Pregnant Women Predict Infant Outcomes following Prenatal Alcohol
1059 Exposure. *PLoS One.* 2016;11(11):e0165081.
1060 12. Rossant J, and Cross JC. Placental development: Lessons from mouse mutants. *Nature Reviews*
1061 *Genetics.* 2001;2:538.
1062 13. E. Davies J, Pollheimer J, Yong HEJ, Kokkinos MI, Kalionis B, Knöfler M, et al. Epithelial-
1063 mesenchymal transition during extravillous trophoblast differentiation. *Cell Adhesion &*
1064 *Migration.* 2016;10(3):310-21.
1065 14. Zhou Y, Damsky CH, and Fisher SJ. Preeclampsia is associated with failure of human
1066 cytotrophoblasts to mimic a vascular adhesion phenotype. One cause of defective endovascular
1067 invasion in this syndrome? *The Journal of Clinical Investigation.* 1997;99(9):2152-64.
1068 15. Damsky CH, and Fisher SJ. Trophoblast pseudo-vasculogenesis: faking it with endothelial
1069 adhesion receptors. *Current opinion in cell biology.* 1998;10(5):660-6.
1070 16. Brown LM, Lacey HA, Baker PN, and Crocker IP. E-cadherin in the assessment of aberrant
1071 placental cytotrophoblast turnover in pregnancies complicated by pre-eclampsia. *Histochemistry*
1072 *and cell biology.* 2005;124(6):499-506.
1073 17. Fedorova L, Gatto-Weis C, Smaili S, Khurshid N, Shapiro JI, Malhotra D, et al. Down-regulation of
1074 the transcription factor snail in the placentas of patients with preeclampsia and in a rat model of
1075 preeclampsia. *Reprod Biol Endocrinol.* 2012;10:15.

1076 18. Blechschmidt K, Mylonas I, Mayr D, Schiessl B, Schulze S, Becker KF, et al. Expression of E-
1077 cadherin and its repressor snail in placental tissue of normal, preeclamptic and HELLP
1078 pregnancies. *Virchows Archiv : an international journal of pathology.* 2007;450(2):195-202.
1079 19. Du L, Kuang L, He F, Tang W, Sun W, and Chen D. Mesenchymal-to-epithelial transition in the
1080 placental tissues of patients with preeclampsia. *Hypertension research : official journal of the*
1081 *Japanese Society of Hypertension.* 2017;40(1):67-72.
1082 20. Gundogan F GJ, Ooi JH, Sung J, Qi W, et al. Dual Mechanisms of Ethanol-Impaired Placentation:
1083 Experimental Model. *J Clin Exp Pathol.* 2013:3:142. doi: 10.4172/2161-0681.1000142.
1084 21. Tai M, Piskorski A, Kao JCW, Hess LA, M. de la Monte S, and Gündoğan F. Placental Morphology
1085 in Fetal Alcohol Spectrum Disorders. *Alcohol and Alcoholism.* 2017;52(2):138-44.
1086 22. Gundogan F, Gilligan J, Qi W, Chen E, Naram R, and de la Monte SM. DOSE EFFECT OF
1087 GESTATIONAL ETHANOL EXPOSURE ON PLACENTATION AND FETAL GROWTH. *Placenta.*
1088 2015;36(5):523-30.
1089 23. Gardebjer EM, Cuffe JS, Pantaleon M, Wlodek ME, and Moritz KM. Periconceptional alcohol
1090 consumption causes fetal growth restriction and increases glycogen accumulation in the late
1091 gestation rat placenta. *Placenta.* 2014;35(1):50-7.
1092 24. Kalisch-Smith JI, Outhwaite JE, Simmons DG, Pantaleon M, and Moritz KM. Alcohol exposure
1093 impairs trophoblast survival and alters subtype-specific gene expression in vitro. *Placenta.*
1094 2016;46:87-91.
1095 25. Bahado-Singh RO, Oz AU, Kingston JM, Shahabi S, Hsu CD, and Cole L. The role of
1096 hyperglycosylated hCG in trophoblast invasion and the prediction of subsequent pre-eclampsia.
1097 *Prenatal diagnosis.* 2002;22(6):478-81.
1098 26. Muller F, Savey L, Le Fiblec B, Bussieres L, Ndayizamba G, Colau JC, et al. Maternal serum human
1099 chorionic gonadotropin level at fifteen weeks is a predictor for preeclampsia. *Am J Obstet*
1100 *Gynecol.* 1996;175(1):37-40.
1101 27. Spencer K, Macri JN, Aitken DA, and Connor JM. Free beta-hCG as first-trimester marker for fetal
1102 trisomy. *Lancet (London, England).* 1992;339(8807):1480.
1103 28. Spencer K. Evaluation of an assay of the free beta-subunit of choriogonadotropin and its
1104 potential value in screening for Down's syndrome. *Clin Chem.* 1991;37(6):809-14.
1105 29. Tsamou M, Vrijens K, Madhloum N, Lefebvre W, Vanpoucke C, and Nawrot TS. Air pollution-
1106 induced placental epigenetic alterations in early life: a candidate miRNA approach. *Epigenetics.*
1107 2018;13(2):135-46.
1108 30. Shi Z, Zhao C, Guo X, Ding H, Cui Y, Shen R, et al. Differential expression of microRNAs in omental
1109 adipose tissue from gestational diabetes mellitus subjects reveals miR-222 as a regulator of
1110 ERalpha expression in estrogen-induced insulin resistance. *Endocrinology.* 2014;155(5):1982-90.
1111 31. McAdams RM, McPherson RJ, Beyer RP, Bammler TK, Farin FM, and Juul SE. Dose-dependent
1112 effects of morphine exposure on mRNA and microRNA (miR) expression in hippocampus of
1113 stressed neonatal mice. *PLoS One.* 2015;10(4):e0123047.
1114 32. Ignacio C, Mooney SM, and Middleton FA. Effects of Acute Prenatal Exposure to Ethanol on
1115 microRNA Expression are Ameliorated by Social Enrichment. *Frontiers in pediatrics.* 2014;2:103.
1116 33. Liu XD, Wu X, Yin YL, Liu YQ, Geng MM, Yang HS, et al. Effects of dietary L-arginine or N-
1117 carbamylglutamate supplementation during late gestation of sows on the miR-15b/16, miR-
1118 221/222, VEGFA and eNOS expression in umbilical vein. *Amino acids.* 2012;42(6):2111-9.
1119 34. Nemoto T, Kakinuma Y, and Shibasaki T. Impaired miR449a-induced downregulation of Crhr1
1120 expression in low-birth-weight rats. *The Journal of endocrinology.* 2015;224(2):195-203.
1121 35. Nardelli C, Granata I, Iaffaldano L, D'Argenio V, Del Monaco V, Maruotti GM, et al. miR-138/miR-
1122 222 Overexpression Characterizes the miRNome of Amniotic Mesenchymal Stem Cells in
1123 Obesity. *Stem cells and development.* 2017;26(1):4-14.

1124 36. Baker BC, Mackie FL, Lean SC, Greenwood SL, Heazell AEP, Forbes K, et al. Placental dysfunction
1125 is associated with altered microRNA expression in pregnant women with low folate status.
1126 *Molecular nutrition & food research.* 2017;61(8).
1127 37. Salihu HM, Kornosky JL, Lynch O, Alio AP, August EM, and Marty PJ. Impact of prenatal alcohol
1128 consumption on placenta-associated syndromes. *Alcohol.* 2011;45(1):73-9.
1129 38. Khong TY. Placental vascular development and neonatal outcome. *Seminars in neonatology : SN.*
1130 2004;9(4):255-63.
1131 39. Ray JG, Vermeulen MJ, Schull MJ, and Redelmeier DA. Cardiovascular health after maternal
1132 placental syndromes (CHAMPS): population-based retrospective cohort study. *Lancet (London,*
1133 *England).* 2005;366(9499):1797-803.
1134 40. Wang D, Na Q, Song WW, and Song GY. Altered Expression of miR-518b and miR-519a in the
1135 placenta is associated with low fetal birth weight. *American journal of perinatology.*
1136 2014;31(9):729-34.
1137 41. Wang JM, Gu Y, Zhang Y, Yang Q, Zhang X, Yin L, et al. Deep-sequencing identification of
1138 differentially expressed miRNAs in decidua and villus of recurrent miscarriage patients. *Archives*
1139 *of gynecology and obstetrics.* 2016;293(5):1125-35.
1140 42. Hromadnikova I, Kotlabova K, Ondrackova M, Pirkova P, Kestlerova A, Novotna V, et al.
1141 Expression profile of C19MC microRNAs in placental tissue in pregnancy-related complications.
1142 *DNA and cell biology.* 2015;34(6):437-57.
1143 43. Hromadnikova I, Kotlabova K, Ivankova K, and Krofta L. Expression profile of C19MC microRNAs
1144 in placental tissue of patients with preterm prelabor rupture of membranes and spontaneous
1145 preterm birth. *Molecular medicine reports.* 2017;16(4):3849-62.
1146 44. Timofeeva AV, Gusar VA, Kan NE, Prozorovskaya KN, Karapetyan AO, Bayev OR, et al.
1147 Identification of potential early biomarkers of preeclampsia. *Placenta.* 2018;61:61-71.
1148 45. Dong F, Zhang Y, Xia F, Yang Y, Xiong S, Jin L, et al. Genome-wide miRNA profiling of villus and
1149 decidua of recurrent spontaneous abortion patients. *Reproduction (Cambridge, England).*
1150 2014;148(1):33-41.
1151 46. Hu Y, Li P, Hao S, Liu L, Zhao J, and Hou Y. Differential expression of microRNAs in the placentae
1152 of Chinese patients with severe pre-eclampsia. *Clinical chemistry and laboratory medicine.*
1153 2009;47(8):923-9.
1154 47. Murphy MS, Casselman RC, Tayade C, and Smith GN. Differential expression of plasma
1155 microRNA in preeclamptic patients at delivery and 1 year postpartum. *Am J Obstet Gynecol.*
1156 2015;213(3):367.e1-9.
1157 48. Bidarimath M, Edwards AK, Wessels JM, Khalaj K, Kridli RT, and Tayade C. Distinct microRNA
1158 expression in endometrial lymphocytes, endometrium, and trophoblast during spontaneous
1159 porcine fetal loss. *Journal of reproductive immunology.* 2015;107:64-79.
1160 49. Gao Y, She R, Wang Q, Li Y, and Zhang H. Up-regulation of miR-299 suppressed the invasion and
1161 migration of HTR-8/SVneo trophoblast cells partly via targeting HDAC2 in pre-eclampsia.
1162 *Biomedicine & pharmacotherapy = Biomedecine & pharmacotherapie.* 2018;97:1222-8.
1163 50. Sandrim VC, Luizon MR, Palei AC, Tanus-Santos JE, and Cavalli RC. Circulating microRNA
1164 expression profiles in pre-eclampsia: evidence of increased miR-885-5p levels. *BJOG : an*
1165 *international journal of obstetrics and gynaecology.* 2016;123(13):2120-8.
1166 51. Rodosthenous RS, Burris HH, Sanders AP, Just AC, Dereix AE, Svensson K, et al. Second trimester
1167 extracellular microRNAs in maternal blood and fetal growth: An exploratory study. *Epigenetics.*
1168 2017;12(9):804-10.
1169 52. Martinez-Fierro ML, Garza-Veloz I, Gutierrez-Arteaga C, Delgado-Enciso I, Barbosa-Cisneros OY,
1170 Flores-Morales V, et al. Circulating levels of specific members of chromosome 19 microRNA

1171 cluster are associated with preeclampsia development. *Archives of gynecology and obstetrics.*
1172 2018;297(2):365-71.
1173 53. Yang S, Li H, Ge Q, Guo L, and Chen F. Deregulated microRNA species in the plasma and placenta
1174 of patients with preeclampsia. *Molecular medicine reports.* 2015;12(1):527-34.
1175 54. Hromadnikova I, Kotlabova K, Ivankova K, and Krofta L. First trimester screening of circulating
1176 C19MC microRNAs and the evaluation of their potential to predict the onset of preeclampsia
1177 and IUGR. *PLOS ONE.* 2017;12(2):e0171756.
1178 55. Zhang M, Muralimanoharan S, Wortman AC, and Mendelson CR. Primate-specific miR-515 family
1179 members inhibit key genes in human trophoblast differentiation and are upregulated in
1180 preeclampsia. *Proceedings of the National Academy of Sciences of the United States of America.*
1181 2016;113(45):E7069-E76.
1182 56. Mei Z, Huang B, Mo Y, and Fan J. An exploratory study into the role of miR-204-5p in pregnancy-
1183 induced hypertension. *Experimental and therapeutic medicine.* 2017;13(5):1711-8.
1184 57. Choi SY, Yun J, Lee OJ, Han HS, Yeo MK, Lee MA, et al. MicroRNA expression profiles in placenta
1185 with severe preeclampsia using a PNA-based microarray. *Placenta.* 2013;34(9):799-804.
1186 58. Kaufmann P, Black S, and Huppertz B. Endovascular trophoblast invasion: implications for the
1187 pathogenesis of intrauterine growth retardation and preeclampsia. *Biol Reprod.* 2003;69(1):1-7.
1188 59. Barrientos G, Pussetto M, Rose M, Staff AC, Blois SM, and Toblli JE. Defective trophoblast
1189 invasion underlies fetal growth restriction and preeclampsia-like symptoms in the stroke-prone
1190 spontaneously hypertensive rat. *Molecular human reproduction.* 2017;23(7):509-19.
1191 60. Roberts JM, and Escudero C. The placenta in preeclampsia. *Pregnancy hypertension.*
1192 2012;2(2):72-83.
1193 61. Fisher SJ. Why is placentation abnormal in preeclampsia? *American journal of obstetrics and*
1194 *gynecology.* 2015;213(4 0):S115-S22.
1195 62. Crosley EJ, Elliot MG, Christians JK, and Crespi BJ. Placental invasion, preeclampsia risk and
1196 adaptive molecular evolution at the origin of the great apes: evidence from genome-wide
1197 analyses. *Placenta.* 2013;34(2):127-32.
1198 63. Lyall F, Bulmer JN, Duffie E, Cousins F, Theriault A, and Robson SC. Human Trophoblast Invasion
1199 and Spiral Artery Transformation : The Role of PECAM-1 in Normal Pregnancy, Preeclampsia, and
1200 Fetal Growth Restriction. *The American Journal of Pathology.* 2001;158(5):1713-21.
1201 64. Goldman-Wohl D, and Yagel S. Regulation of trophoblast invasion: from normal implantation to
1202 pre-eclampsia. *Molecular and cellular endocrinology.* 2002;187(1-2):233-8.
1203 65. Balaraman S, Lunde ER, Sawant O, Cudd TA, Washburn SE, and Miranda RC. Maternal and
1204 neonatal plasma microRNA biomarkers for fetal alcohol exposure in an ovine model. *Alcohol Clin*
1205 *Exp Res.* 2014;38(5):1390-400.
1206 66. Panwar B, Omenn GS, and Guan Y. miRmine: a database of human miRNA expression profiles.
1207 *Bioinformatics.* 2017;33(10):1554-60.
1208 67. Vicovac L, and Aplin JD. Epithelial-mesenchymal transition during trophoblast differentiation.
1209 *Acta anatomica.* 1996;156(3):202-16.
1210 68. Knöfler M, and Pollheimer J. Human placental trophoblast invasion and differentiation: a
1211 particular focus on Wnt signaling. *Frontiers in Genetics.* 2013;4:190.
1212 69. Arimoto-Ishida E, Sakata M, Sawada K, Nakayama M, Nishimoto F, Mabuchi S, et al. Up-
1213 regulation of alpha5-integrin by E-cadherin loss in hypoxia and its key role in the migration of
1214 extravillous trophoblast cells during early implantation. *Endocrinology.* 2009;150(9):4306-15.
1215 70. Sun YY, Lu M, Xi XW, Qiao QQ, Chen LL, Xu XM, et al. Regulation of epithelial-mesenchymal
1216 transition by homeobox gene DLX4 in JEG-3 trophoblast cells: a role in preeclampsia.
1217 *Reproductive sciences (Thousand Oaks, Calif).* 2011;18(11):1138-45.

1218 71. Barrak J, Msheik H, Abou-Kheir W, and Daoud G. Assessment of different trophoblast cell lines
1219 as in vitro models for placental development. *Placenta.* 2016;45:106.
1220 72. Lovisa S, LeBleu VS, Tampe B, Sugimoto H, Vadnagara K, Carstens JL, et al. Epithelial-to-
1221 mesenchymal transition induces cell cycle arrest and parenchymal damage in renal fibrosis.
1222 *Nature medicine.* 2015;21(9):998-1009.
1223 73. Vega S, Morales AV, Ocana OH, Valdes F, Fabregat I, and Nieto MA. Snail blocks the cell cycle
1224 and confers resistance to cell death. *Genes & development.* 2004;18(10):1131-43.
1225 74. Kolahi KS, Valent AM, and Thornburg KL. Cytotrophoblast, Not Syncytiotrophoblast, Dominates
1226 Glycolysis and Oxidative Phosphorylation in Human Term Placenta. *Scientific Reports.*
1227 2017;7:42941.
1228 75. Lu X, He Y, Zhu C, Wang H, Chen S, and Lin HY. Twist1 is involved in trophoblast syncytialization
1229 by regulating GCM1. *Placenta.* 2016;39:45-54.
1230 76. Omata W, Ackerman WEIV, Vandre DD, and Robinson JM. Trophoblast Cell Fusion and
1231 Differentiation Are Mediated by Both the Protein Kinase C and A Pathways. *PLOS ONE.*
1232 2013;8(11):e81003.
1233 77. Moreau R, Hamel A, Daoud G, Simoneau L, and Lafond J. Expression of calcium channels along
1234 the differentiation of cultured trophoblast cells from human term placenta. *Biol Reprod.*
1235 2002;67(5):1473-9.
1236 78. Spaans F, Melgert BN, Chiang C, Borghuis T, Klok PA, de Vos P, et al. Extracellular ATP decreases
1237 trophoblast invasion, spiral artery remodeling and immune cells in the mesometrial triangle in
1238 pregnant rats. *Placenta.* 2014;35(8):587-95.
1239 79. Karl PI, Chusid J, Tagoe C, and Fisher SE. Ca2+ flux in human placental trophoblasts. *Am J Physiol.*
1240 1997;272(6 Pt 1):C1776-80.
1241 80. Roberts VH, Waters LH, and Powell T. Purinergic receptor expression and activation in first
1242 trimester and term human placenta. *Placenta.* 2007;28(4):339-47.
1243 81. Halmesmaki E, Autti I, Granstrom ML, Stenman UH, and Ylikorkala O. Estradiol, estriol,
1244 progesterone, prolactin, and human chorionic gonadotropin in pregnant women with alcohol
1245 abuse. *J Clin Endocrinol Metab.* 1987;64(1):153-6.
1246 82. Edelstam G, Karlsson C, Westgren M, Lowbeer C, and Swahn ML. Human chorionic gonadatropin
1247 (hCG) during third trimester pregnancy. *Scandinavian journal of clinical and laboratory*
1248 *investigation.* 2007;67(5):519-25.
1249 83. Soares MJ, Chakraborty D, Rumi MAK, Konno T, and Renaud SJ. Rat Placentation: An
1250 Experimental Model For Investigating The Hemochorial Maternal-Fetal Interface. *Placenta.*
1251 2012;33(4):233-43.
1252 84. Grigsby PL. Animal Models to Study Placental Development and Function throughout Normal
1253 and Dysfunctional Human Pregnancy. *Seminars in reproductive medicine.* 2016;34(1):11-6.
1254 85. Vercruysse L, Caluwaerts S, Luyten C, and Pijnenborg R. Interstitial trophoblast invasion in the
1255 decidua and mesometrial triangle during the last third of pregnancy in the rat. *Placenta.*
1256 2006;27(1):22-33.
1257 86. Silva JF, and Serakides R. Intrauterine trophoblast migration: A comparative view of humans and
1258 rodents. *Cell Adhesion & Migration.* 2016;10(1-2):88-110.
1259 87. Kurtzman JT, Wilson H, and Rao CV. A Proposed Role for hCG in Clinical Obstetrics. *Semin Reprod*
1260 *Med.* 2001;19(01):063-8.
1261 88. Furcron A-E, Romero R, Mial TN, Balancio A, Panaitescu B, Hassan SS, et al. Human Chorionic
1262 Gonadotropin Has Anti-Inflammatory Effects at the Maternal-Fetal Interface and Prevents
1263 Endotoxin-Induced Preterm Birth, but Causes Dystocia and Fetal Compromise in Mice. *Biology of*
1264 *Reproduction.* 2016;94(6):136.

1265 89. Henderson GI, Hoyumpa AM, Jr., McClain C, and Schenker S. The effects of chronic and acute
1266 alcohol administration on fetal development in the rat. *Alcohol Clin Exp Res.* 1979;3(2):99-106.
1267 90. O'Leary-Moore SK, Parnell SE, Godin EA, Dehart DB, Ament JJ, Khan AA, et al. Magnetic
1268 resonance microscopy-based analyses of the brains of normal and ethanol-exposed fetal mice.
1269 *Birth Defects Res A Clin Mol Teratol.* 2010;88(11):953-64.
1270 91. Lo JO, Schabel MC, Roberts VH, Wang X, Lewandowski KS, Grant KA, et al. First trimester alcohol
1271 exposure alters placental perfusion and fetal oxygen availability affecting fetal growth and
1272 development in a non-human primate model. *Am J Obstet Gynecol.* 2017;216(3):302.e1-.e8.
1273 92. Bake S, Tingling JD, and Miranda RC. Ethanol exposure during pregnancy persistently attenuates
1274 cranially directed blood flow in the developing fetus: evidence from ultrasound imaging in a
1275 murine second trimester equivalent model. *Alcohol Clin Exp Res.* 2012;36(5):748-58.
1276 93. Gaccioli F, and Lager S. Placental Nutrient Transport and Intrauterine Growth Restriction.
1277 *Frontiers in Physiology.* 2016;7:40.
1278 94. Haggarty P, Abramovich DR, and Page K. The effect of maternal smoking and ethanol on fatty
1279 acid transport by the human placenta. *The British journal of nutrition.* 2002;87(3):247-52.
1280 95. Lui S, Jones RL, Robinson NJ, Greenwood SL, Aplin JD, and Tower CL. Detrimental Effects of
1281 Ethanol and Its Metabolite Acetaldehyde, on First Trimester Human Placental Cell Turnover and
1282 Function. *PLOS ONE.* 2014;9(2):e87328.
1283 96. Rufer ES, Tran TD, Attridge MM, Andrzejewski ME, Flentke GR, and Smith SM. Adequacy of
1284 Maternal Iron Status Protects against Behavioral, Neuroanatomical, and Growth Deficits in Fetal
1285 Alcohol Spectrum Disorders. *PLoS ONE.* 2012;7(10):e47499.
1286 97. Huebner SM, Blohowiak SE, Kling PJ, and Smith SM. Prenatal Alcohol Exposure Alters Fetal Iron
1287 Distribution and Elevates Hepatic Hepcidin in a Rat Model of Fetal Alcohol Spectrum Disorders.
1288 *The Journal of Nutrition.* 2016;146(6):1180-8.
1289 98. Xie L, Mouillet J-F, Chu T, Parks WT, Sadovsky E, Knöfler M, et al. C19MC MicroRNAs Regulate
1290 the Migration of Human Trophoblasts. *Endocrinology.* 2014;155(12):4975-85.
1291 99. Salomon C, Torres MJ, Kobayashi M, Scholz-Romero K, Sobrevia L, Dobierzewska A, et al. A
1292 Gestational Profile of Placental Exosomes in Maternal Plasma and Their Effects on Endothelial
1293 Cell Migration. *PLOS ONE.* 2014;9(6):e98667.
1294 100. Ouyang Y, Mouillet J-F, Coyne CB, and Sadovsky Y. Placenta-specific microRNAs in exosomes –
1295 good things come in nano-packages. *Placenta.* 2014;35 Suppl:S69-S73.
1296 101. Sabapatha A, Gercel-Taylor C, and Taylor DD. Specific isolation of placenta-derived exosomes
1297 from the circulation of pregnant women and their immunoregulatory consequences. *American*
1298 *journal of reproductive immunology (New York, NY : 1989).* 2006;56(5-6):345-55.
1299 102. Nair S, and Salomon C. Extracellular vesicles and their immunomodulatory functions in
1300 pregnancy. *Seminars in immunopathology.* 2018.
1301 103. Delorme-Axford E, Donker RB, Mouillet J-F, Chu T, Bayer A, Ouyang Y, et al. Human placental
1302 trophoblasts confer viral resistance to recipient cells. *Proceedings of the National Academy of*
1303 *Sciences of the United States of America.* 2013;110(29):12048-53.
1304 104. Donker RB, Mouillet JF, Chu T, Hubel CA, Stolz DB, Morelli AE, et al. The expression profile of
1305 C19MC microRNAs in primary human trophoblast cells and exosomes. *Molecular human*
1306 *reproduction.* 2012;18(8):417-24.
1307 105. Cronqvist T, Tannetta D, Mörgelin M, Belting M, Sargent I, Familari M, et al. Syncytiotrophoblast
1308 derived extracellular vesicles transfer functional placental miRNAs to primary human endothelial
1309 cells. *Scientific Reports.* 2017;7(1):4558.
1310 106. Smith SM, Garic A, Flentke GR, and Berres ME. Neural Crest Development in Fetal Alcohol
1311 Syndrome. *Birth defects research Part C, Embryo today : reviews.* 2014;102(3):210-20.

1312 107. Kalcheim C. Epithelial–Mesenchymal Transitions during Neural Crest and Somite Development.
1313 *Journal of Clinical Medicine.* 2016;5(1):1.
1314 108. Yang J, Qiu H, Qu P, Zhang R, Zeng L, and Yan H. Prenatal Alcohol Exposure and Congenital Heart
1315 Defects: A Meta-Analysis. *PLoS ONE.* 2015;10(6):e0130681.
1316 109. Burd L, Deal E, Rios R, Adickes E, Wynne J, and Klug MG. Congenital heart defects and fetal
1317 alcohol spectrum disorders. *Congenital heart disease.* 2007;2(4):250-5.
1318 110. Serrano M, Han M, Brinez P, and Linask KK. Fetal alcohol syndrome: cardiac birth defects in mice
1319 and prevention with folate. *Am J Obstet Gynecol.* 2010;203(1):75.e7-.e15.
1320 111. Sarmah S, and Marrs JA. Complex cardiac defects after ethanol exposure during discrete
1321 cardiogenic events in zebrafish: Prevention with folic acid. *Developmental dynamics : an official*
1322 *publication of the American Association of Anatomists.* 2013;242(10):1184-201.
1323 112. Combs MD, and Yutzey KE. Heart Valve Development: Regulatory networks in development and
1324 disease. *Circulation research.* 2009;105(5):408-21.
1325 113. Lin C-J, Lin C-Y, Chen C-H, Zhou B, and Chang C-P. Partitioning the heart: mechanisms of cardiac
1326 septation and valve development. *Development (Cambridge, England).* 2012;139(18):3277-99.
1327 114. Janssen HL, Reesink HW, Lawitz EJ, Zeuzem S, Rodriguez-Torres M, Patel K, et al. Treatment of
1328 HCV infection by targeting microRNA. *The New England journal of medicine.* 2013;368(18):1685-
1329 94.
1330 115. Beg MS, Brenner AJ, Sachdev J, Borad M, Kang YK, Stoudemire J, et al. Phase I study of MRX34, a
1331 liposomal miR-34a mimic, administered twice weekly in patients with advanced solid tumors.
1332 *Invest New Drugs.* 2017;35(2):180-8.
1333 116. Sathyan P, Golden HB, and Miranda RC. Competing interactions between micro-RNAs determine
1334 neural progenitor survival and proliferation after ethanol exposure: evidence from an ex vivo
1335 model of the fetal cerebral cortical neuroepithelium. *J Neurosci.* 2007;27(32):8546-57.
1336 117. Huang W, Tian SS, Hang PZ, Sun C, Guo J, and Du ZM. Combination of microRNA-21 and
1337 microRNA-146a Attenuates Cardiac Dysfunction and Apoptosis During Acute Myocardial
1338 Infarction in Mice. *Molecular therapy Nucleic acids.* 2016;5:e296.
1339 118. Brady ML, Allan AM, and Caldwell KK. A Limited Access Mouse Model of Prenatal Alcohol
1340 Exposure that Produces Long-Lasting Deficits in Hippocampal-Dependent Learning and Memory.
1341 *Alcoholism, clinical and experimental research.* 2012;36(3):457-66.
1342 119. Kajimoto K, Allan A, and Cunningham LA. Fate Analysis of Adult Hippocampal Progenitors in a
1343 Murine Model of Fetal Alcohol Spectrum Disorder (FASD). *PLoS ONE.* 2013;8(9):e73788.
1344 120. Watson ED, and Cross JC. Development of structures and transport functions in the mouse
1345 placenta. *Physiology (Bethesda).* 2005;20:180-93.
1346 121. Gårdebjer EM, Anderson ST, Pantaleon M, Wlodek ME, and Moritz KM. Maternal alcohol intake
1347 around the time of conception causes glucose intolerance and insulin insensitivity in rat
1348 offspring, which is exacerbated by a postnatal high-fat diet. *The FASEB Journal.* 2015;29(7):2690-
1349 701.
1350 122. Grant KA, Leng X, Green HL, Szeliga KT, Rogers LS, and Gonzales SW. Drinking typography
1351 established by scheduled induction predicts chronic heavy drinking in a monkey model of
1352 ethanol self-administration. *Alcohol Clin Exp Res.* 2008;32(10):1824-38.
1353 123. Carter AM. Animal models of human placentation--a review. *Placenta.* 2007;28 Suppl A:S41-7.
1354 124. Orendi K, Gauster M, Moser G, Meiri H, and Huppertz B. The choriocarcinoma cell line BeWo:
1355 syncytial fusion and expression of syncytium-specific proteins. *Reproduction (Cambridge,*
1356 *England).* 2010;140(5):759-66.
1357 125. Oh SY, Hwang JR, Lee Y, Choi SJ, Kim JS, Kim JH, et al. Isolation of basal membrane proteins from
1358 BeWo cells and their expression in placentas from fetal growth-restricted pregnancies. *Placenta.*
1359 2016;39:24-32.

1360 126. Schindelin J, Arganda-Carreras I, Frise E, Kaynig V, Longair M, Pietzsch T, et al. Fiji: an open-
1361 source platform for biological-image analysis. *Nature methods.* 2012;9(7):676-82.
1362 127. Gong J, Wu Y, Zhang X, Liao Y, Sibanda VL, Liu W, et al. Comprehensive analysis of human small
1363 RNA sequencing data provides insights into expression profiles and miRNA editing. *RNA biology.*
1364 2014;11(11):1375-85.

1365